Segregation of Ni and Si to coherent bcc Fe-Cu interfaces from density functional theory

DOI:
https://doi.org/10.1016/j.jnucmat.2021.153185

Document Version
Final published version

Journal of Nuclear Materials 556 (2021) 153185

Contents lists available at ScienceDirect

Journal of Nuclear Materials

journal homepage: www.elsevier.com/locate/jnucmat

Segregation of Ni and Si to coherent bcc Fe-Cu interfaces from density functional theory

A.M. Garrett, C.P. Race*

Department of Materials, University of Manchester, Manchester, UK

ARTICLE INFO

Article history:
Received 16 April 2021
Revised 5 July 2021
Accepted 6 July 2021
Available online 7 July 2021

Keywords:
Density functional theory
Pressure vessel steel
Solute segregation
Coherent interfaces
Embrittlement
Precipitates

ABSTRACT

The formation of Cu rich precipitates (CRPs) is known to substantially contribute to the embrittlement of reactor pressure vessel steels with high Cu contents. CRPs are commonly observed to possess a Cu core surrounded by a shell of other segregating solute species like Mn, Ni and Si. Here we calculate the segregation energies of substitutional Ni and Si to {100}, {110} and {111} orientated coherent Fe-Cu interfaces. We find Ni is strongly attracted to all orientations of coherent bcc Fe-Cu interfaces whilst Si interacts in a more complex manner, with strong attraction only to the {100} orientation. In calculating these segregation energies we also explore different methods, concluding that for this system using an external reference bulk (ERB) is optimal. By performing additional calculations we were able to decouple the elastic and chemical contributions to segregation energy finding that for Ni the chemical contributions dominate whilst for Si the two contributions are more balanced. In conjunction with previous work we conclude that should Cu nanoprecipitate sizes influence segregation behaviours it is likely this will not be due to the strain state surrounding the Cu nanoprecipitate. It is more probable that this size dependence would originate from variation in the proportions of the specific orientations of coherent Fe-Cu interface that make up the Cu nanoprecipitate's surface at different sizes.

1. Introduction

The presence of Cu, and its interaction with other solute elements, in low-alloy reactor pressure vessel (RPV) steels has been known to contribute towards the component's embrittlement for decades [1,2]. During a pressurised water reactor's (PWR) operation the RPV is exposed to elevated temperatures and neutron irradiation leading to changes in its microstructure. Atom probe tomography (APT) commonly observes the formation of Cu rich precipitates (CRPs) which are seen to possess an almost pure Cu core surrounded by a shell of other solute elements, typically Mn, Ni and Si [3–10]. Such core-shell morphologies are also predicted through Monte Carlo and thermodynamic modelling methods [11–14]. The formation of CRPs, as well as MnNiSi precipitates (MNSPs), is thought to substantially contribute to RPV embrittlement by their acting as barriers to dislocation movement. This embrittlement is typically observed in Charpy-V impact tests where significant shifts in the ductile-to-brittle transition temperatures (DBTT) and upper shelf energy of RPV steels are seen following periods of elevated temperature and neutron irradiation [10,15,16]. The RPV is a safety critical component and so understanding the processes that lead to its embrittlement is important in assessing the operating limits of the component over its lifetime.

Given the core-shell morphology of CRPs, it has been suggested that the coherent interface between Fe and Cu, that makes up the surface of the Cu nanoprecipitate core region, may be acting as a site of segregation for the other solute species (Mn, Ni and Si) that make up the CRP [6,17]. This interface may then assist in the formation of a large solute enriched region which surrounds the Cu nanoprecipitate core region [13,18]. It is proposed these large solute enriched regions could then function as formation sites for complex precipitate phases [17,19–22] that some suggest may lead to anomalous late-life embrittlement of the RPV [23]. This anomalous late-life embrittlement is of considerable interest as it is thought to be poorly represented in current embrittlement models. As such, the formation of these MnNiSi-rich complex precipitate phases could represent a significant barrier to extending the lifetime of a PWR. Whilst historically RPV steel compositions were relatively high in Cu, more modern alloys have much stricter tolerances on its presence (< 0.05 at.%). However, even at such low concentrations it is possible the Cu present may still partially contribute to late-life RPV embrittlement by assisting the formation

* Corresponding author.
E-mail address: christopher.race@manchester.ac.uk (C.P. Race).

https://doi.org/10.1016/j.jnucmat.2021.153185

of MnNiSi-rich regions [17] which may then evolve into complex precipitate phases.

In this work we focus on coherent interfaces between bcc Cu and the bcc Fe matrix. High resolution electron microscopy studies of Cu precipitates in thermally aged α-Fe shows that below 4 nm in diameter these precipitates remain in the bcc phase, coherent with the matrix [24]. Evidence from irradiation studies using pressure vessel steels and model alloys suggests that under irradiation the CRPs formed typically remain below this size [7,8,25,26] suggesting that coherent interfaces are the appropriate model. Evidence from modelling studies suggests that vacancies play an important role in the diffusion of Cu and the formation of CRPs [27–30]. It is plausible, therefore, that CRPs have a finite vacancy content. In the present work we focus on perfect interfaces and neglect the presence of vacancies. Including the effects of co-segregation of multiple species, including vacancies, to the interfaces adds considerable complexity to the picture and we will address these effects separately in a future paper.

In this work we use Fe-Cu interfaces simulated with density functional theory (DFT) to investigate the segregation behaviours of Ni and Si. By constructing simulation cells containing {100}, {110} and {111} orientated Fe-Cu interfaces and substituting solute species of interest into these cells we can explore the influence of interface orientation and solute species on segregation. Within the literature there are two predominant methods used to calculate segregation energy, using either an internal reference bulk (IRB) [31–36] or external reference bulk (ERB) [37–41] as defined in Section 2. Whilst both IRB and ERB methods have their advantages and proponents, it is often unclear which method represents best practice for a given system. In this work we perform segregation energy calculations for Ni to all three orientations of Fe-Cu interface using both IRB and ERB calculations. Through this testing on the Ni system we identify the ERB calculations as our preferred method and then apply it to the case of Si segregation. We initially explore the influence of interfacial solute concentration on the segregation energies of Ni and Si allowing us to identify a simulation cell size at which we can consider the interfacial solute concentration to be effectively dilute. We then use this interfacial solute concentration dilute limit as a basis for investigating the influence of bulk solute concentration on segregation. Finally, we performed additional calculations that enable us to decouple the segregation energy contributions associated with the strain state and chemistry of the interface site.

We performed further calculations in which the interface-containing simulation cells were strained parallel (ϵ_{x-y}) and perpendicular (ϵ_z) to the Fe-Cu interface, using the ERB method. The periodic nature of the simulation cells requires us to ensure that artificial strain states present in the simulation cells are not leading to unrealistic segregation energies. By straining the simulation cells and calculating new segregation energies it is possible to gain confidence that the findings are not excessively influenced by the constraints on the system and gain further insights into the role strain plays in solute segregation. Our previous work used an embedded atom method (EAM) potential [42] to investigate how the size of a Cu nanoprecipitate influences the strain in the plane of Fe-Cu interface (ϵ_{x-y}) [43]. By observing how these predicted strains alter the calculated segregation energy we can infer the influence of Cu nanoprecipitate size on solute segregation behaviour. The process of straining the simulation cells also allows us to learn about how strain more broadly influences segregation behaviour, i.e. do the solute species prefer compressive or tensile environments.

Whilst we initially focus on calculating the segregation of Ni and Si to the interface plane itself, we further use our ERB method to calculate the segregation energies of Ni and Si to additional sites near to the interface. One would expect that interactions between the interface and segregating solute would be strongest when the solute is at a site on the interface. However, this is not necessarily the case and sites near to, but not on, the interface may prove more energetically favourable.

2. Methods

As mentioned, literature describes two primary methods by which segregation energies are calculated using an internal reference bulk (IRB) and an external reference bulk (ERB). Fundamentally, both methods of calculating segregation energy rely on the comparison of a system's ground-state energy with the solute species of interest at a site on the interface and at a site distant from the interface. It is this site which is distant from the interface, and therefore considered to be reference bulk, where the distinction between the two methods exists. Within this work in all cases it is an Fe atom that is substituted for solute.

In this section we will describe the parameters and methods used to perform these segregation energy calculations. The techniques used to decouple the elastic and chemical contributions to calculated segregation energy will also be discussed. We further explain how the simulation cells were transformed in order to explore the influence of simulation cell constraint and interfacial strain on our segregation energy calculations. Finally we describe the methods used to calculate the equilibrium interface solute occupancies.

2.1. Density functional theory (DFT) parameters

All simulations in this work were performed using density functional theory (DFT), an ab initio quantum mechanical simulation method. These DFT calculations were implemented in VASP 5.4.4 [44] on the University of Manchester's Computational Shared Facility (CSF). All the calculations described below used projector augmented wave (PAW) pseudopotentials [45] with the Perdew, Burke and Eisenhof generalised gradient approximation (GGA-PBE) [46] used for the exchange-correlation (XC) functional. The Fe pseudopotential treats 8 ($3d^7\ 4s^1$) electrons as valence, the Cu pseudopotential treats 11 ($3d^{10}\ 4s^1$) electrons as valence, the Ni pseudopotential treats 10 ($3d^8\ 4s^2/3d^9\ 4s^1$) electrons as valence and the Si pseudopotential treats 4 ($3s^2\ 3p^2$) electrons as valence. All calculations were spin polarised using collinear magnetism with initial spins for Fe set to 3.0 μ_B, Cu set to 0.0 μ_B, Ni set to 1.0 μ_B and Si set to set to -1.0 μ_B. Methfessel-Paxton smearing [47] was used with $\sigma = 0.15$eV. In all cases ionic relaxations were performed with the dimensions of the simulation cells kept fixed. The total energy convergence criterion for the self-consistent loop was set to 10^{-5} eV whilst the convergence criterion for the ionic relaxations was set to 10^{-4} eV.

For both segregation energy calculation methods we use the convention that negative values correspond to attraction, i.e. there is a reduction in energy associated with solute moving from the bulk to the interface. Conversely, positive segregation energies indicate solute atom is repelled by the interface.

2.2. Internal reference bulk (IRB)

The IRB method calculates segregation energy as

$$E^{\mathrm{I,IRB}}_{\mathrm{seg,i}} = E^{\mathrm{FeICu}}_{\mathrm{i}} - E^{\mathrm{FeICu}}_{\mathrm{b}}, \quad (1)$$

where $E^{\mathrm{I,IRB}}_{\mathrm{seg,i}}$ is the calculated segregation energy of solute I to an on-interface site (an example of which is shown in cell 1a from Fig. 1), $E^{\mathrm{FeICu}}_{\mathrm{i}}$ is the ground-state energy of simulation cell 1a where an Fe atom at the interface is substituted for a solute atom and $E^{\mathrm{FeICu}}_{\mathrm{b}}$ is the ground-state energy of simulation cell 1b (also shown in Fig. 1) where an Fe atom is substituted for a solute atom

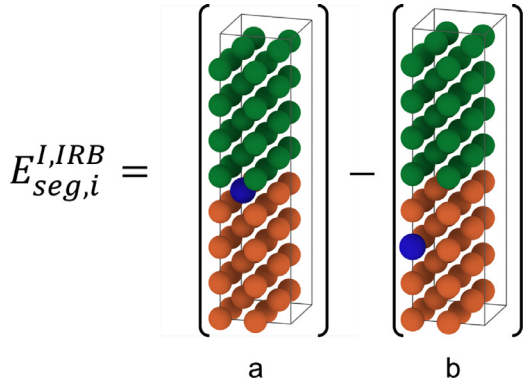

Fig. 1. Example simulation cells required to calculate segregation energy using the IRB method where the Fe atoms are in orange, the Cu atoms are in green and the segregating solute species is in blue. (For interpretation of the references to colour in this figure legend, the reader is referred to the web version of this article.)

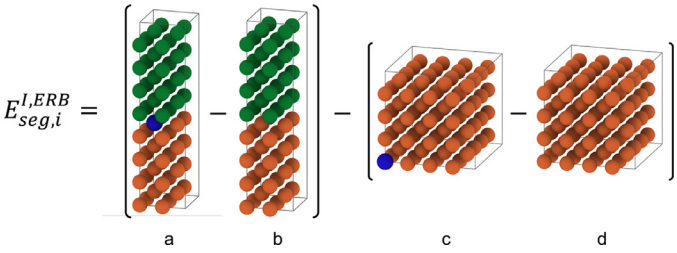

Fig. 2. Example simulation cells required to calculate segregation energy using the ERB method where the Fe atoms are in orange, the Cu atoms are in green and the segregating species is in blue. (For interpretation of the references to colour in this figure legend, the reader is referred to the web version of this article.)

in the reference bulk Fe region, which is taken to be the site furthest from the interface. What we aim to calculate with Eq. (1) is the change in energy associated with a solute atom moving from bulk Fe (a site infinitely distant from a Cu nanoprecipitate) to a site at the Fe-Cu interface (the surface of our Cu nanoprecipitate). In this case our reference bulk Fe is a site inside a simulation cell containing an interface, hence the name *internal reference bulk*. Here we require that the substituted solute atom is beyond the effective interaction range of the interface so that it can be treated as if it were truly in bulk Fe and thus infinitely distant from the interface. One proposed advantage of this method is that because the solute atoms have identical separations from their periodic repeats when at the interface and reference bulk sites then the error introduced by solute-solute interactions will be cancelled allowing for the use of smaller solute spacings in the plane of the interface.

2.3. External reference bulk

The ERB method calculates segregation energy as

$$E^{\mathrm{I,ERB}}_{\mathrm{seg,i}} = (E^{\mathrm{FeICu}}_{\mathrm{i}} - E^{\mathrm{FeCu}}_{\mathrm{i}}) - (E^{\mathrm{FeI}}_{\mathrm{B}} - E^{\mathrm{Fe}}_{\mathrm{B}}), \quad (2)$$

where $E^{\mathrm{I,ERB}}_{\mathrm{seg,i}}$ is the segregation energy of solute I using the ERB method, $E^{\mathrm{FeICu}}_{\mathrm{i}}$ is the ground-state energy of simulation cell 2a (shown in Fig. 2) where an Fe atom at the interface is substituted for a solute atom, $E^{\mathrm{FeCu}}_{\mathrm{i}}$ is the ground-state energy of simulation cell 2b with no substitution at the interface, $E^{\mathrm{FeI}}_{\mathrm{B}}$ is the ground-state energy of simulation cell 2c where an Fe atom in the bulk Fe simulation cell is substituted for a solute atom and $E^{\mathrm{Fe}}_{\mathrm{B}}$ is the ground-state energy of simulation cell 2d with no substitution in the bulk Fe. Here we similarly aim to calculate the change in energy associated with a solute atom moving from a site within bulk Fe to a site at the Fe-Cu interface. Whilst in the IRB method we use a region of our interface-containing simulation cell to act as our reference bulk Fe, here in the ERB method we use a separate simulation cell, *external* to the one which contains the interface to act as our reference bulk Fe. In order to conserve the quantities of each species in the calculation it is necessary to subtract from each solute-containing simulation cell (2a and 2c) an equivalent simulation cell which is solute-free (cells 2b and 2d). We can consider the first expression in brackets from Eq. (2) to effectively be the energy associated with swapping an Fe atom for a solute atom at the interface and the second expression in brackets to be the energy associated with swapping an Fe atom for a solute atom in the reference bulk Fe. One advantage of the ERB method is that we should be able to use shorter simulation cells in the direction normal to the interface since it is only the interfacial region that needs to be well represented. However, this method does require four calculations to be performed per segregation system though the reference bulk values can be re-used. A further advantage of the ERB method is that it allows us to effectively explore how interfacial and bulk solute concentration (C_I and C_B respectively) influence segregation behaviour. For example, if we use a reference bulk cell that contains $2 \times 2 \times 2$ bcc Fe unit cells then we have 16 Fe atoms. When we substitute one of those Fe atoms for a solute atom then we have an effective bulk solute concentration of $1/16 = 6.25$ at.%. Table A.1 shows the reference bulk Fe simulation cell sizes used and their corresponding bulk solute concentrations.

Within the ERB method we also decouple the chemical and elastic contributions to the calculated segregation energy. Whilst there are several ways to quantify this distinction, in this method we opted to do so by first relaxing the ionic positions of simulation cells 2a and 2c. We then take these ionic positions as an input for a second calculation were we substitute the solute out of the relaxed simulation cell and replace it with Fe. We can then calculate the ground state energy of these simulation cells which are effectively strained as if a solute atom were in them but without the solute atom present, which we denote as $E^{\mathrm{FeI'Cu}}_{\mathrm{i}}$ for the interface-containing simulation cell (2a) and $E^{\mathrm{FeI'}}_{\mathrm{B}}$ for the reference bulk simulation cell (2c). We can then write the elastic contribution to segregation energy as

$$E^{\mathrm{I,ERB}}_{\mathrm{seg,el}} = (E^{\mathrm{FeI'Cu}}_{\mathrm{i}} - E^{\mathrm{FeCu}}_{\mathrm{i}}) - (E^{\mathrm{FeI'}}_{\mathrm{B}} - E^{\mathrm{Fe}}_{\mathrm{B}}). \quad (3)$$

Clearly the chemical contribution must make up what remains of the total segregation energy, $E^{\mathrm{I,ERB}}_{\mathrm{seg,i}}$ giving the expression for the chemical contribution:

$$E^{\mathrm{I,ERB}}_{\mathrm{seg,ch}} = (E^{\mathrm{FeICu}}_{\mathrm{i}} - E^{\mathrm{FeI'Cu}}_{\mathrm{i}}) - (E^{\mathrm{FeI}}_{\mathrm{B}} - E^{\mathrm{FeI'}}_{\mathrm{B}}). \quad (4)$$

2.4. Cut-off energy and k point density convergence

Simulation cells were fixed to a DFT derived Fe lattice parameter of 0.283 nm as in previous work [43]. Cut-off energy and k point density convergence studies were performed with a 16 atom {100} orientated Fe-Cu interface with Ni only for the IRB method and with both Ni and Si for the ERB method. A k point density equivalent to a $16 \times 16 \times 16$ Monkhorst-Pack (MP) grid [48] for a bcc Fe unit cell and 400 eV cut-off energy gave segregation energies converged to < 0.01 eV in all cases. In some cases it is not possible to achieve exact k point equivalence due to geometrical constraints, in which case the MP grid was chosen to give as similar values to the ideal case as possible.

2.5. Solute separation and interfacial spacing convergence

When performing segregation energy calculations with an interface we find the two most difficult parameters to converge are the solute separation and interfacial spacing. Due to the periodically repeating nature of the simulation cell there will be effec-

Table 1
Simulation cell lengths and interfacial solute concentrations required for C_I dilute limit segregation energy calculations for Ni and Si with the convergence tolerances they provide.

Species	Orientation	Cell length (atoms)	Conv. tol. (eV)	C_I (at · nm^{-2})	Conv. tol. (eV)
Ni	{100}	16	0.01	1.38	0.03
	{110}	32	0.02	2.20	0.03
	{111}	24	0.01	1.80	0.02
Si	{100}	16	0.03	1.38	0.05
	{110}	32	0.02	2.20	0.01
	{111}	24	0.03	1.80	0.02

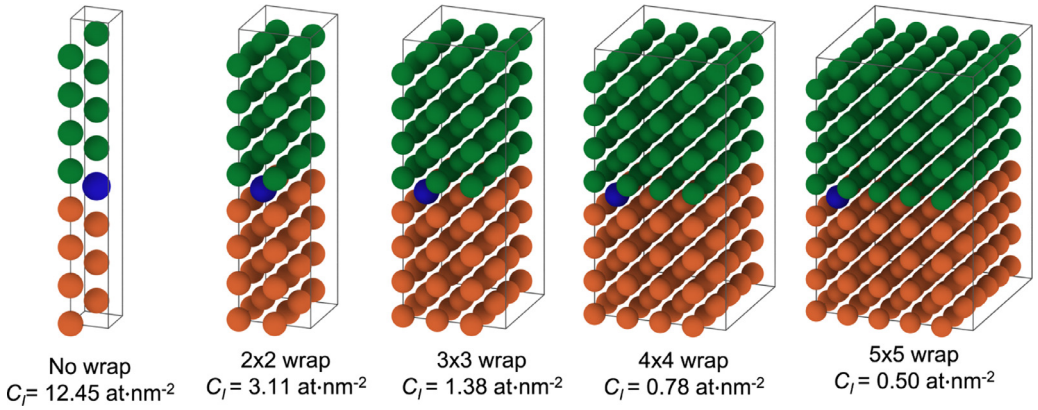

Fig. 3. Example wrapped simulation cells containing {100} orientated Fe-Cu interfaces. The 2×2 wrap nomenclature refers to the number of columns in each direction parallel to the interface used to make up the simulation cell. The equivalent effective interfacial solute concentrations (C_I) are also shown.

tively two interfaces within it. It is thus important to ensure that the spacing between those two interfaces is sufficiently large that any solute elements substituted into the simulation cell are interacting with one interface at most. This interfacial spacing convergence can be tested by calculating the segregation energy of a solute element in increasingly long simulation cells (in the direction normal to the interface) until increasing the length of the simulation cell no longer significantly alters the segregation energy calculated. For Ni this testing was performed for all interface orientations using both the IRB and ERB calculation methods with the simulation cell lengths from Table A.2 given in Appendix A). For Si this testing was only performed using the ERB method but again using the cell lengths given in Table A.2.

Similarly, the periodically repeating nature of the simulation cells means that any substituted solute element will interact with its periodic repeats in the directions perpendicular and parallel to the interface. Given the previously discussed requirements for interfacial spacing, our simulation cells are sufficiently long that the solute-solute interactions in the direction perpendicular to the interface are negligible. Parallel to the interface the solute-solute separation is much smaller. To counter this interaction the solute-containing simulation cell can be wrapped in near identical solute-free interface-containing columns of atoms to increase the distance between the solute atom and its periodic repeats in the plane of the interface. This process additionally reduces the effective interface solute concentration (C_I), measured as the number of atoms per unit area. Whilst we are primarily interested in calculating segregation energies at the dilute limit with respect to interfacial solute concentration, we can also learn about the relationship between interfacial solute concentration and segregation energy during this process. Examples of these wrapped simulation cells are shown in Fig. 3 with their effective interface solute concentrations labelled. Table A.3 (in Appendix A) details the interfacial solute concentration along with the number of simulation cells in the x and y directions to create the wrapped simulation cell. In this work we calculate the change in segregation energy with decreasing interface solute concentration for all interface orientations to find the dilute limit which we then use in all studies not focussed on the influence of interfacial solute concentration. Both Ni and Si use the same interfacial solute concentrations as the dilute limit.

2.6. Strained interfaces

As previously mentioned, by straining the interface-containing simulation cells we can simultaneously explore the influence of Cu nanoprecipitate size on segregation energy and also ensure artificial strains induced by our chosen dimensions of simulation cell aren't excessively contributing to the segregation behaviours we observe. Within the framework of ERB segregation energy calculations we found the segregation energy values for both Ni and Si to all three orientations of Fe-Cu interfaces. The interface-containing simulation cells were strained to −3%, −2%, −1%, 0%, 1%, 2% and 3% in the plane of the interface ($x-y$ directions) in the first strain study. In the second strain study the interface-containing simulation cells were deformed perpendicular to the interface (z direction) to strains of 0%, 1%, 2%, 3%, 4%, 5% and 6%. In both strain studies the simulation cells were strained and then the ionic positions were allowed to relax whilst the dimensions of the simulation cells were held fixed.

2.7. Interface-adjacent segregation

In addition to the segregation site directly on the interface, we have also chosen to calculate the segregation energies of both Ni and Si to sites adjacent to the interface. These segregation energies are calculated again using the ERB method except that in this case the E_i^{FeICu} term represents the ground-state energy of a simulation cell with solute sitting at one of interface-adjacent sites illustrated in Fig. 4. All interface-adjacent sites used in this study for the {100}, {110} and {111} orientated Fe-Cu interfaces are shown also in Fig. 4 where site 1 represents the on-interface solute position. It is important to note that the sites for each interface orientation are not equivalent, i.e. site 2 in the {110} cell is not the same position as site 2 in the {111}. The numbering of the sites

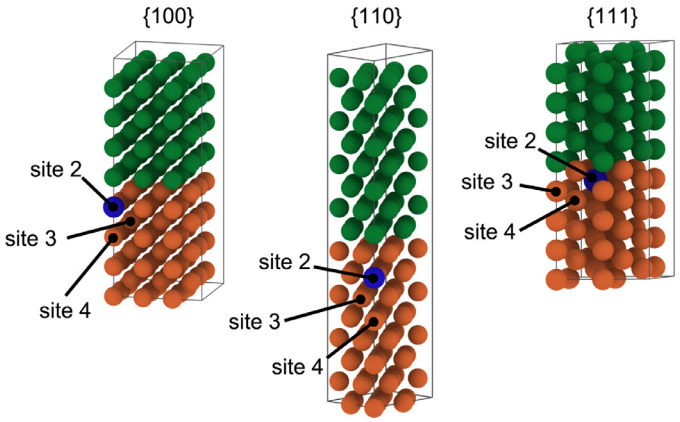

Fig. 4. Plots illustrate the additional sites to which solute was substituted in the interface-adjacent site study for simulation cells containing {100}, {110} and {111} orientated Fe-Cu interfaces. Fe is depicted in orange, Cu in green and the substitutional solute atom in blue. In these examples the solute atom is substituted into site 2 for all Fe-Cu interface orientations. (For interpretation of the references to colour in this figure legend, the reader is referred to the web version of this article.)

refers to the atomic layer on which the site sits with respect to the interface, i.e. site 2 is on the second atomic layer back from the interface.

2.8. Equilibrium interface solute occupancy

Having calculated the segregation energies of Ni and Si to effectively dilute interfaces for all three orientations at a range of effective bulk solute concentrations using the ERB method, we are then able to use the Langmuir-McLean binary isotherm equation [49–51] to calculate the influence of temperature on the equilibrium solute occupancy (i.e. the fraction of sites on the interface occupied by solute).

3. Results and discussion

In this section we present our comparison of segregation energy calculation methods, the solute segregation energies we calculate, the influence of strain on segregation energy and the Langmuir-McLean binary isotherm findings. We will further discuss the implications of these findings in the context of solute segregation to different morphologies of Cu nanoprecipitates.

3.1. Reference bulk comparison

Here we present our results regarding the comparison of the IRB and ERB segregation energy calculation methods when applied to the segregation of Ni to all three orientations of Fe-Cu interface. We initially show the difference in response to increasing interfacial spacing and decreasing interfacial solute concentration. We then justify our use of one method over the other for this particular application. In this comparison the ERB method results use a bulk Ni concentration of 0.40 at.%.

Figure 5 shows the calculated segregation energy for increasing interfacial spacing to all three interface orientations using both segregation energy calculation techniques, IRB and ERB. The ERB method is relatively insensitive to interfacial spacing suggesting using longer, more computationally expensive, simulation cells is unnecessary. In contrast, the IRB method requires much longer simulation cells to achieve similar levels of convergence. For example, to achieve a convergence tolerance of < 0.01 eV for Ni segregation to a {100} orientated Fe-Cu interface the IRB method requires a cell containing at least 32 atoms whilst for the ERB method 16 atoms are sufficient. It is worth noting that the IRB and ERB methods do not converge to the same value with increasing interfacial spacing because the two methods are not necessarily converged with respect to interfacial solute concentration or bulk solute concentration for the simulation cell sizes used, as discussed below.

Figure 6 shows the influence of interface solute concentration (C_I) on the calculated segregation energy. We plot this as C_I^{-1} so that as the x axis values increase we approach the dilute limit we wish to converge towards. Simulation cell lengths for the interfacial solute concentration convergence study were chosen to be as short as possible whilst still giving good interfacial spacing convergence for the ERB calculation method (i.e. 16, 32 and 24 atoms for the {100}, {110} and {111} orientation respectively) to reduce computational costs. Again, we would not expect the two methods to converge to the same segregation energy value in this study because the IRB method is not converged with respect to interfacial spacing whilst the ERB method is. For this interfacial solute concentration study the relative superiority of one method over the other is less distinct. It does appear that for an equivalent interfacial concentration a tighter convergence tolerance is provided by the IRB method compared to the ERB method. Again, this is well illustrated by the {100} interface. An interfacial Ni concentration of 1.38 at $\cdot$ nm^{-2} ($C_I^{-1} = 0.72$ at$^{-1} \cdot$ nm^2)) gives a convergence tolerance for the IRB method of < 0.02 eV, narrower than the convergence tolerance for the ERB method of < 0.03 eV. It is important to clarify that one should only expect the IRB and ERB methods to produce equivalent segregation energies when both methods are converged with respect to interfacial separation, interfacial solute concentration and bulk solute concentration.

Since the ERB method gives improved convergence at smaller interfacial spacings and the two methods offer similar convergence with respect to interfacial solute concentration, we conclude that the ERB method will provide equivalent results to the IRB method but using smaller simulation cells (reducing computational costs). The ability to more directly explore the influence of interfacial (C_I) and bulk solute concentration (C_B) further strengthens the case for using the ERB method.

As previously mentioned, it is logical the IRB method would require simulation cells with larger interfacial spacings because it is necessary for a region of bulk-like Fe to be present between the interface regions. When we look at how the energy of the solute (cell 1b in Fig. 1) in this internal reference bulk region varies with interfacial spacing it becomes clear that it is this energy contribution which inhibits convergence for smaller simulation cells. We can re-write the IRB segregation energy calculation as

$$E_{\mathrm{seg,i}}^{\mathrm{I,IRB}} = E_{\mathrm{seg,i}}^{\mathrm{I,ERB}} - E_{\mathrm{seg,b}}^{\mathrm{I,ERB}} \tag{5}$$

where $E_{\mathrm{seg,i}}^{\mathrm{I,ERB}}$ and $E_{\mathrm{seg,b}}^{\mathrm{I,ERB}}$ are the segregation energies of solute I to the solute sites shown in cells 1a and 1b respectively using the ERB method. A derivation of Eq. (5) is given in Appendix B. If we then plot $E_{\mathrm{seg,i}}^{\mathrm{I,ERB}}$ and $-E_{\mathrm{seg,b}}^{\mathrm{I,ERB}}$ (as shown in Fig. 7) it becomes clear that the contribution associated with the bulk-like site in the IRB method ($E_{\mathrm{seg,b}}^{\mathrm{I,ERB}}$) converges more slowly than the contribution of the interface site ($E_{\mathrm{seg,i}}^{\mathrm{I,ERB}}$). Clearly the ERB method doesn't suffer from this limitation because it is only necessary for the interface region to be converged. Similarly, it is logical that the IRB method should have improved performance in the solute spacing study due to the cancellation of solute-solute interactions introduced by interactions between the solute and its periodic images. However, such solute-solute interaction cancellation would also make studying the influence of interfacial solute concentration on segregation energy complicated.

To calculate the segregation energy of a single solute to a single interface, the ERB method requires four calculations (as expressed in Eq. (2)) where the IRB method needs only two (as expressed in Eq. (1)). However, in wider studies like ours, this extra expense

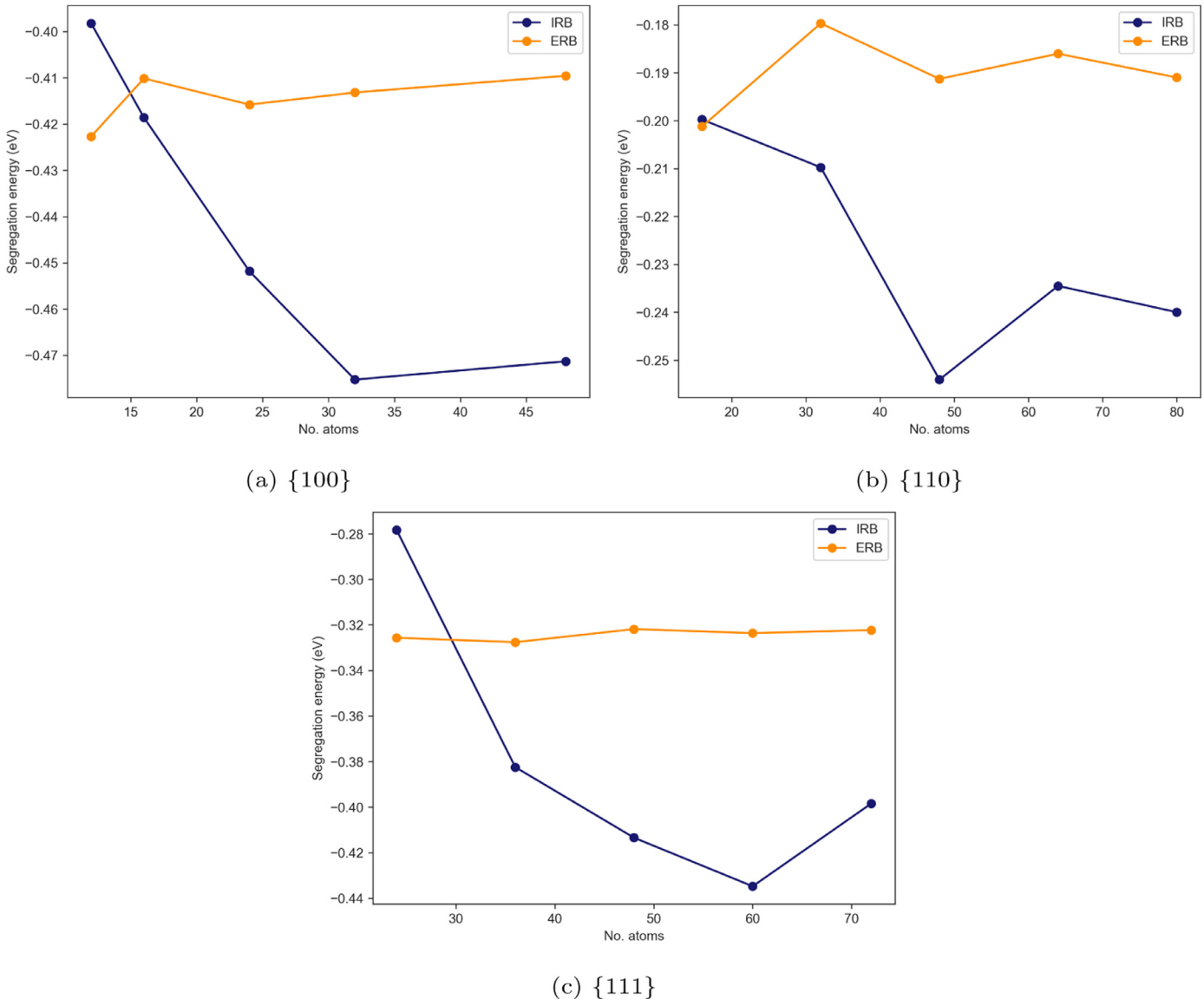

Fig. 5. Plots show the variation in calculated segregation energy for Ni to each interface orientation for increasing simulation cell length using both the IRB and ERB segregation energy calculation methods.

is offset by the fact that the energies of the solute-free interfaces, $E_{\mathrm{i}}^{\mathrm{FeCu}}$, can be reused in treating multiple solutes and the energies of the bulk reference, $E_{\mathrm{B}}^{\mathrm{FeI}}$ and $E_{\mathrm{B}}^{\mathrm{Fe}}$, can be used across multiple interface orientations.

3.2. Solute segregation energies

Having identified the advantages of using the external reference bulk (ERB) method for this system, we then performed segregation energy calculations for Ni and Si to all three Fe-Cu interface orientations. We initially explored the influence of interface solute concentration (C_I) where the concentrations used are shown in Table A.3. We identified interface solute concentrations of 1.38, 2.20 and 1.80 at $\cdot$ nm^{-2} to be effectively the dilute limit for the {100}, {110} and {111} orientated Fe-Cu interfaces. At C_I values below these the calculated segregation energies fall within relatively narrow convergence tolerances ($<$ 0.05 eV in all cases) as shown in Table 1. Simulation cells at the dilute limit with respect to C_I were then used to explore the influence of bulk solute concentration (C_B) on the segregation energies of Ni and Si to effectively dilute Fe-Cu interfaces. The simulation cell parameters and the convergence they provide with respect to segregation energy for these bulk solute concentration segregation studies are shown in Table 1. For these bulk solute concentration segregation studies we also applied the decoupling method described in Section 2.3 to separate the elastic and chemical energy contributions for solute segregating to an effectively dilute interface.

3.2.1. Dependence on interfacial solute concentration

Figure 8 a illustrates the relationship between interfacial solute concentration and segregation energy. In the case of Ni, this relationship is relatively pronounced for segregation to the {100} orientation demonstrating more attractive segregation energies to interfaces containing less solute whilst interfaces with higher solute concentrations see less attractive segregation energies. This broadly suggests that as solute segregates to the Cu nanoprecipitate, surface regions with the {100} orientation will become less attractive to segregating Ni as they become increasingly decorated with Ni. Generally, the segregation of Ni to the {110} and {111} orienta-

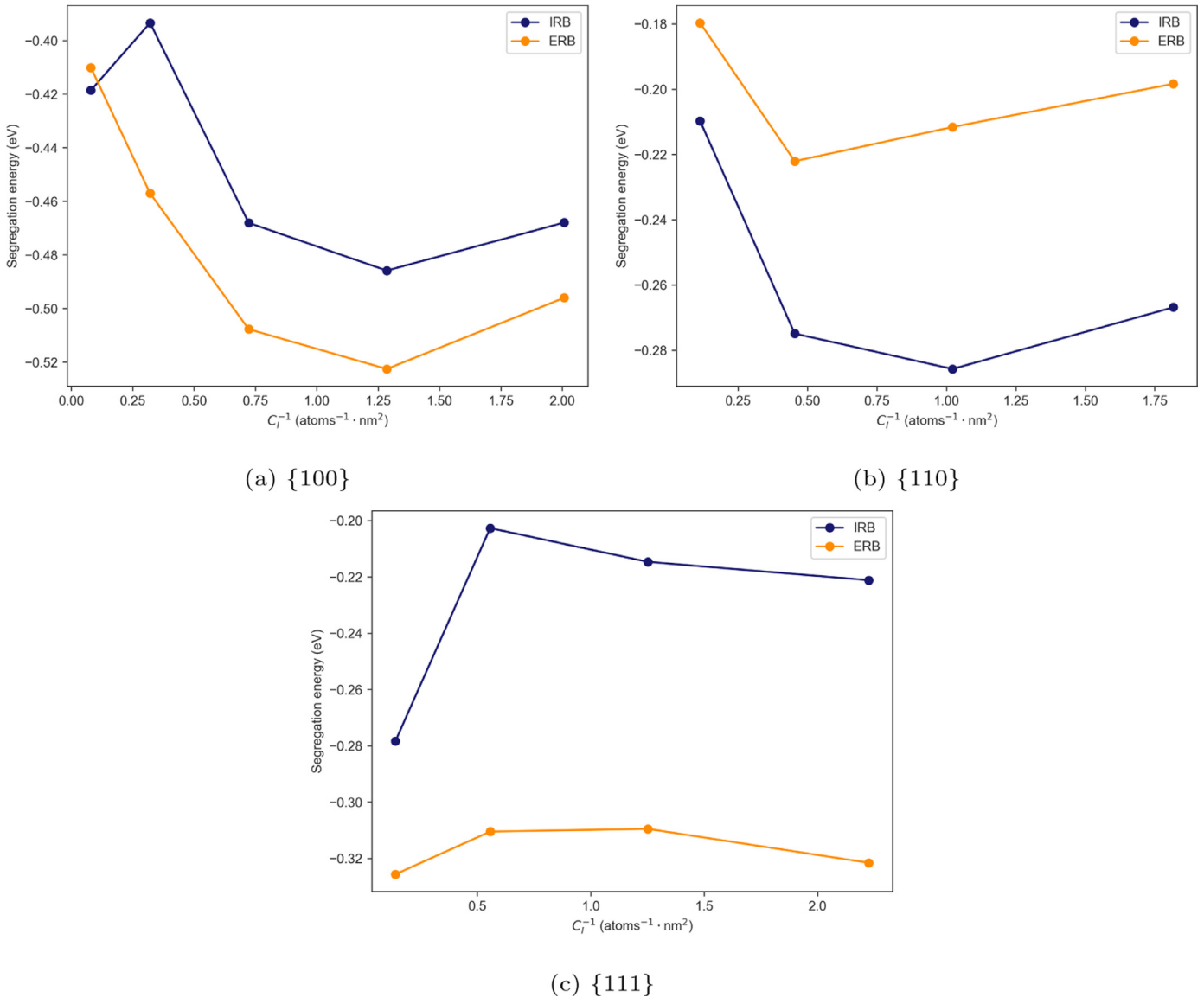

Fig. 6. Plots show the variation in calculated segregation energy for Ni to each interface orientation for decreasing interfacial solute concentration (C_I) using both the IRB and ERB segregation energy calculation methods.

tions is largely independent of interfacial solute concentration for the solute concentrations investigated in this work. This suggests that the potential energy of Ni segregation to these two interfaces will be relatively constant during the initial stages of segregation where solute segregates primarily to on-interface sites. Our prior work [43] shows these two orientations are relatively low energy and are thus more likely to form the surface of the Cu nanoprecipitate.

Figure 8 b shows the relationship between Si interfacial concentration and segregation energy. As for Ni, Si segregation exhibits little dependence on interfacial solute concentration for the {110} and {111} orientations whilst the {100} orientation exhibits a greater dependence. However, at the highest interfacial solute concentrations the {100} and {110} orientations both become substantially less attractive to Si segregation. These findings further demonstrate that, regardless of interfacial solute concentration, Si will not be attracted to the on-interface segregation site (i.e. site 1) for the {111} orientated interface. Early in the segregation process the {100} and {110} orientated interfaces will have little Si present on the interface and so will be attractive to segregating Si. However, as the solute concentration of the interface increases and the Si atoms come to sit at second nearest neighbour sites, the repulsive Si-Si interactions at this separation may dominate [29,52]. This suggests the capacity for Cu nanoprecipitates to attract Si to on-interface segregation sites is limited by the available surface with relatively low Si concentrations and {100}/{110} orientated Fe-Cu interfaces. Our previous work [43] demonstrates the {100} orientated Fe-Cu interface is comparatively high energy and so is unlikely to form in large proportions of the Cu nanoprecipitates' surfaces further limiting how attractive they are to Si. In these interface solute concentration studies we used a bulk solute concentration of 0.40 at.% for both Ni and Si as in the convergence studies.

3.2.2. Dependence on bulk solute concentration

Figure 9 a plots the segregation energy against bulk Ni concentration (C_B) for the {100}, {110} and {111} orientated Fe-Cu interfaces at the dilute limit for interfacial Ni concentration. The influence of bulk Ni concentration on segregation energy is relatively small and the use of a bulk Ni concentration elsewhere in this work of 0.40 at.% is chosen for consistency. This suggests bulk Ni

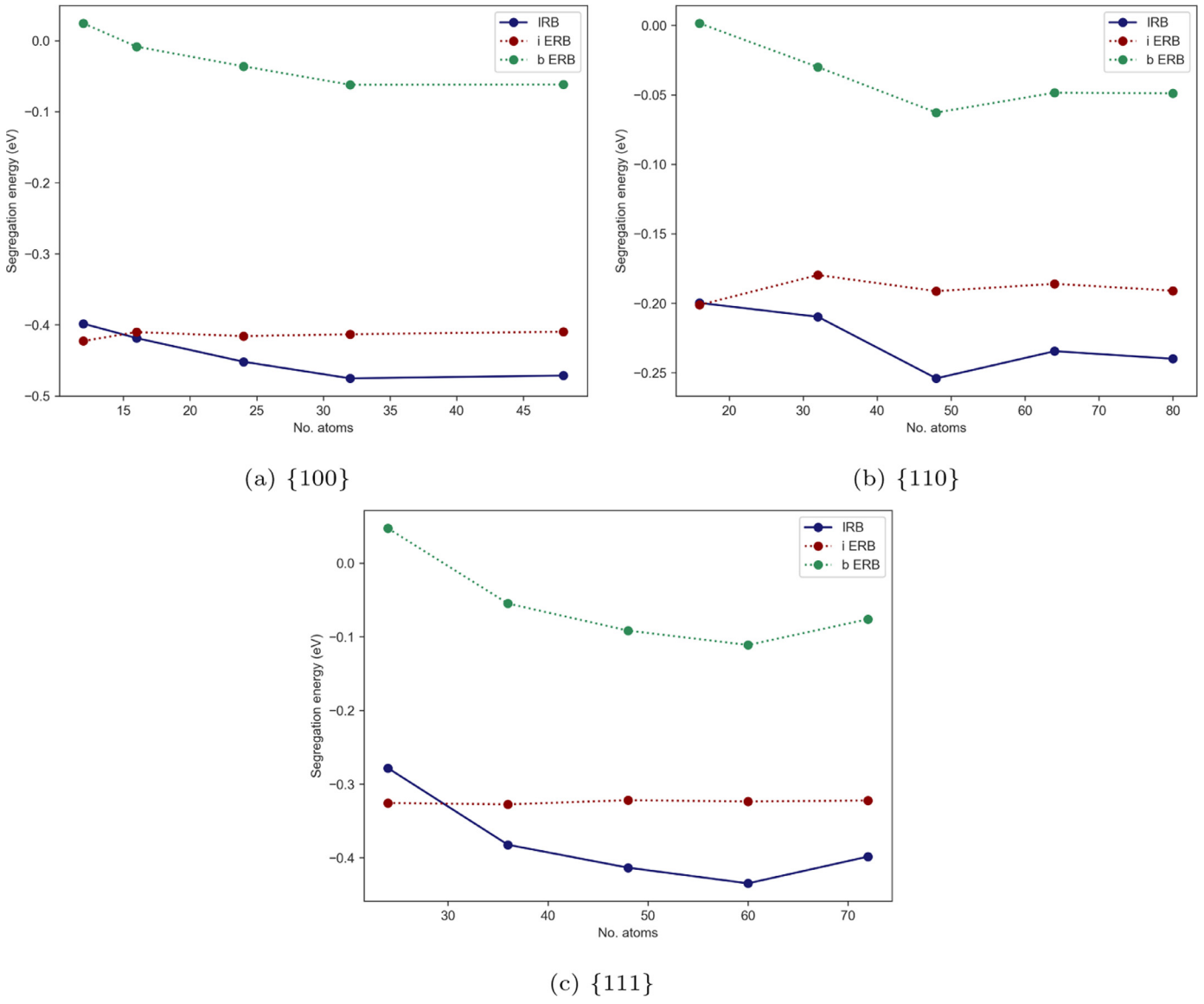

Fig. 7. Plots show the contribution to the IRB calculated Ni segregation energy from the simulation cells with solute in the bulk-like region and solute in the interface region.

concentration does not substantially alter the potential energy of Ni segregation to Fe-Cu interfaces especially when compared to the much stronger dependence of segregation energy on interface orientation at the concentrations tested. The attraction of Ni to {100} orientated Fe-Cu interfaces is strongest, with segregation energy values of approximately −0.50 eV. This value is in good agreement with the work of Xie et al. (2012) [31] who found the segregation energy of Ni to a {100} orientated Fe-Cu interface using an IRB method to be −0.44 eV. The {111} orientation is the second most attractive with segregation energy values of around −0.30 eV whilst the {110} orientation is the least attractive of the three with values around −0.20 eV. Our previous work [43] suggested that Cu nanoprecipitate surfaces should predominantly be made up of {110} orientated Fe-Cu interfaces but as the nanoprecipitates increase in size other orientations are more likely to feature in the surface. It can be inferred that larger Cu nanoprecipitates are likely to produce a stronger driving force for Ni segregation given that Ni is more strongly attracted to non-{110} interface orientations.

In Fig. 9b the elastic and chemical contributions to segregation energy for Ni are plotted separately. We can immediately see that the elastic contribution for the three interface orientations is exceptionally small. Conversely, the chemical contribution seemingly makes up the vast majority of Ni's segregation energy. This finding is in good agreement with the work of Xie et al. [31] where they too find Ni segregation to the {100} orientated Fe-Cu interface is dominated by chemical considerations. Whilst the distinction between elastic and chemical contributions is somewhat artificial given the interconnectedness of strain state and bond length, we can conclude that Ni is attracted to Fe-Cu interfaces not because of the strain state that exists in this region but instead because of the different bonds that it forms.

Similarly, Fig. 9b shows the segregation energy of Si plotted against its bulk concentration, again for the {100}, {110} and {111} orientated Fe-Cu interfaces at the dilute limit for interfacial Si concentration. In the case of Si the relationship between bulk concentration and segregation energy seems to be stronger, demonstrating a weak trend that segregation becomes more attractive (i.e. more -ve) as bulk Si concentration increases. Whiting et al. [29] and Bakaev et al. [52] both demonstrate relatively strong Si-Si repulsion in bulk Fe at the first and second nearest neighbour (1nn and 2nn respectively) positions with this interaction becoming mildly attractive at the 3nn, 4nn and 5nn positions.

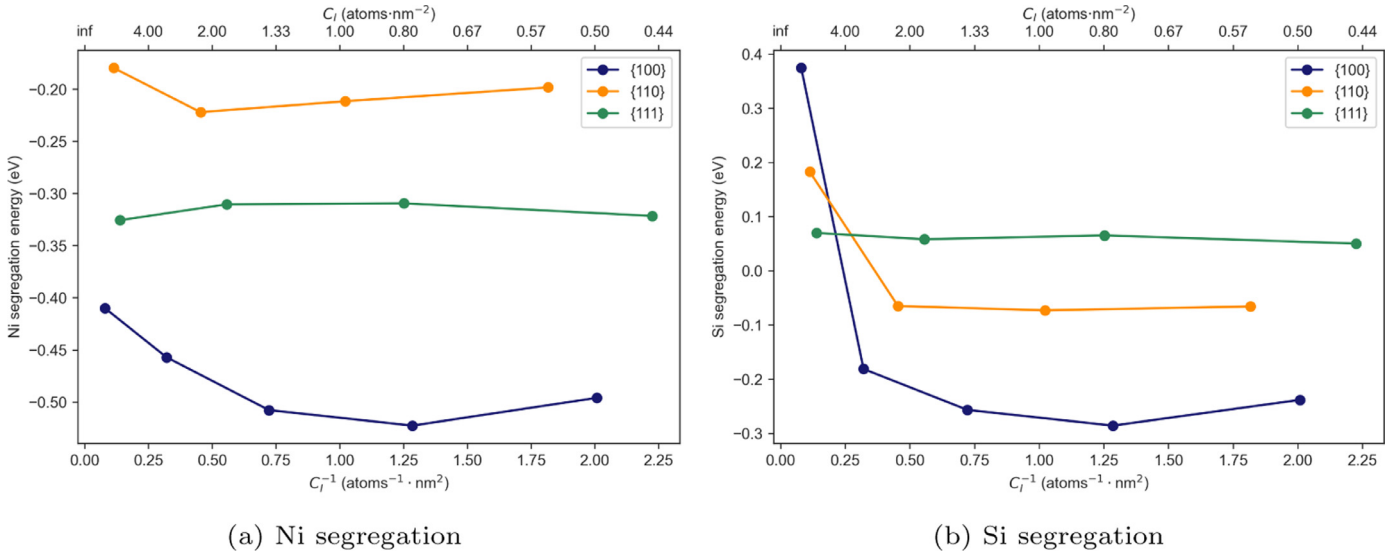

Fig. 8. Variation in calculated segregation energy with decreasing Ni (left) and Si (right) interfacial solute concentrations (C_I) to each interface orientation. Left plot shows the variation in calculated segregation energy with decreasing Si interface solute concentration to each interface orientation. The bulk solute concentration in both cases is 0.40 at.%.

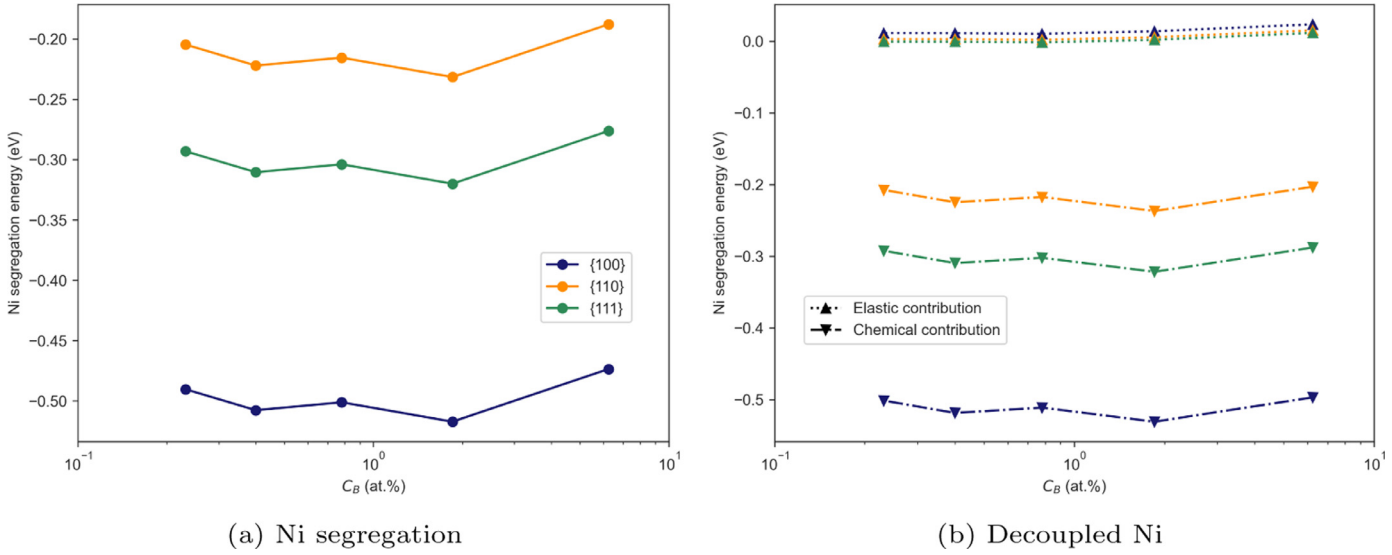

Fig. 9. Left plot shows the variation in calculated segregation energy to each interface orientation for increasing bulk solute concentration of Ni. Right plot shows the variation in elastic and chemical contributions to segregation energy to each interface orientation. Upward pointing triangles represent the elastic contribution whilst downward pointing arrows represent the chemical contribution.

Given that even at the highest bulk Si concentrations investigated the Si atoms are at 6nn positions, this attractive interaction would need to be quite long ranged to explain the reductions in segregation energy observed. However, it is possible the weak trend of more attractive segregation with increasing bulk concentration may result from a comparatively long ranged elastic repulsion becoming dominated by the shorter ranged chemical attraction as the bulk Si concentration increases and the distance between the Si atoms decreases. Though, it is also possible this trend stems from error in the calculation given these variations in segregation energy are within our expected convergence tolerances. Whilst the effect of changing interface orientation on Si segregation energies is similar in magnitude to the case for Ni (approx. 0.1–0.3 eV), this results in a qualitative change in segregation behaviour for Si. Whilst Si exhibits a moderately strong attraction to the {100} orientated Fe-Cu interface (approx. −0.25 eV) it is weakly repelled by the {111} orientated interface (approx. +0.05 eV). Finally, the Si seems to be only weakly attracted to the {110} orientation (approx. −0.07 eV). Xie and Zhao [32] calculated the segregation energy of Si to a {100} orientated Fe-Cu interface to be −0.03 eV using an IRB method, a value substantially smaller in magnitude than the one we calculate. This disparity is possibly due to their use of the IRB calculation method or may result from their use of smaller supercells and hence higher interfacial concentrations. These explanations are partially supported by the observation in our ERB method interfacial solute concentration studies which indicate smaller solute-solute spacings result in more repulsive segregation interactions. The more complex dependence of Si segregation on interface orientation means that the relationship between broader Si segregation behaviours and Cu nanoprecipitate size may also be more complex. If the non-{110} surfaces of larger Cu nanoprecipitate possesses the {100} orientation we may expect elevated Si segregation whereas if the non-{110} interfaces have the {111} orientation we might expect reduced Si segregation. It is possible

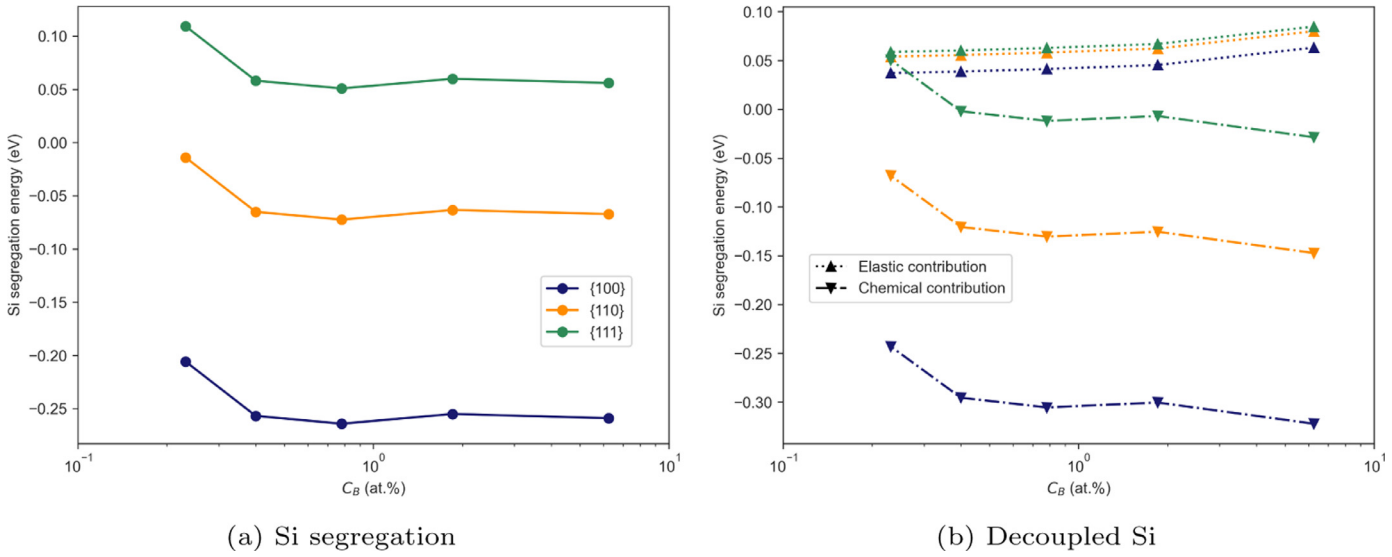

Fig. 10. Left plot shows the variation in calculated segregation energy to each interface orientation for increasing bulk solute concentration of Si. Right plot shows the variation in elastic and chemical contributions to segregation energy to each interface orientation. Upward pointing triangles represent the elastic contribution whilst downward pointing arrows represent the chemical contribution.

that small regions of {100} orientated interface could result in a localised Si enrichment possibly contributing to appendage-like morphologies [8,13,17,53].

Figure 10b shows the decoupled elastic and chemical contributions to segregation energy for Si. Whilst for the {100} orientated interface the majority of the attraction Si experiences is due to the chemical contribution, the contribution of strain is stronger than for Ni and repulsive. Similarly, the weak attraction of Si to the {110} orientated Fe-Cu interface is made up of a relatively strong attractive chemical component and a weaker repulsive elastic component. Finally, in the case of the {111} orientated interface the repulsive elastic component overcomes the weaker attractive chemical component resulting in the total weak repulsion observed. Whilst Ni's interaction with the interface was primarily chemical in nature, the interaction of Si is more subtle and depends on the balance struck between elastic and chemical effects.

The magnitude of Si's interaction with Fe-Cu interfaces is smaller than that of Ni. As such, we might expect greater Ni segregation to a Cu nanoprecipitate. However, the driving force for segregation is only part of the process and the ease with which both species can diffuse through Fe could also significantly influence the solute concentration of the interface region. Versteylen et al. [54] calculated the diffusion constant (D_0) and activation energy (Q) for diffusion of Ni and Si in bcc ferromagnetic Fe using DFT assuming predominantly single vacancy diffusion. For Ni they found $D_0 = 3.6 \times 10^{-5}$ $m^2 \cdot s^{-1}$ and $Q = 2.656$ eV, comparing favourably with experimental values of Hirano et al. [55] and Borg and Lai [56]. For Si they obtained $D_0 = 3.6 \times 10^{-5}$ $m^2 \cdot s^{-1}$ and $Q = 2.570$ eV, seeing weaker agreement with the experimental findings of Bergner et al. [57]. Given the similarity in the diffusion constants and activation energies for Ni and Si, the stronger segregation energies of Ni are likely to be the dominant factor in determining the segregation behaviour. However, we note that it is possible that the diffusion of the two solute species will be differently affected by neutron irradiation when vacancies will be relatively abundant given Si is seen to bond more strongly to divacancy triplets compared to Ni [29].

As previously mentioned, CRPs are sometimes observed to possess MnNiSi-rich appendage structures [8,13,17,53]. We can see that if a small region of {100} interface were to form on the surface of a Cu nanoprecipitate then this region may preferentially attract any available solute, helping to form a localised region of enrichment due to the strong segregation of both Ni and Si to the {100} interface. Though, as we see in Fig. 8a and b the {100} orientated interface becomes less attractive to Ni as the Ni concentration increases and becomes repulsive to Si as the Si concentration increases. However, in order to make more conclusive comments about this locally preferential segregation it is necessary to further investigate how Ni and Si interact with each other in the interfacial region to establish how energetically favourable it is for solute to segregate to interfaces that are already decorated with similar and dissimilar species of solute. It may well be the case that the solute enriched region more effectively draws in solute compared to the undecorated Fe-Cu interface.

3.3. Influence of strain

Figures 11 a and 12 a show how the segregation energies of Ni and Si vary with applied $x-y$ strains, i.e. in the interfacial plane. For both segregating species, there is a significant dependence of calculated segregation energy on $x-y$ plane strain in the {100} orientated interface, with both species demonstrating a preference for segregating to interfaces in compression. For Si this preference for compressive $x-y$ plane strains is also demonstrated for the {110} and {111} orientations whilst for Ni there is very little variation for these non-{100} orientations.

Figures 11 b and 12 b similarly show the variations of Ni and Si segregation energies with applied z strain, i.e. acting perpendicular to the interface. For both species the {100} and {111} orientations the calculated segregation energies are largely unaffected by the z strain, though there seems to be a weak preference for more compressive z strains in the {100} orientation and more tensile z strains in the {111} orientation. However, the segregation energies for both species to the {110} orientation do demonstrate a strong dependence on z strain. This behaviour is a consequence of the Cu atoms in the simulation cell moving to off-bcc lattice positions. These shifts in position significantly reduce the calculated ground state energy of the simulation cell and it appears that by straining the {110} orientated interface in this way and introducing an asymmetry in the form of a solute substitutional we are assisting the transformation of Cu from a bcc to its equilibrium fcc structure.

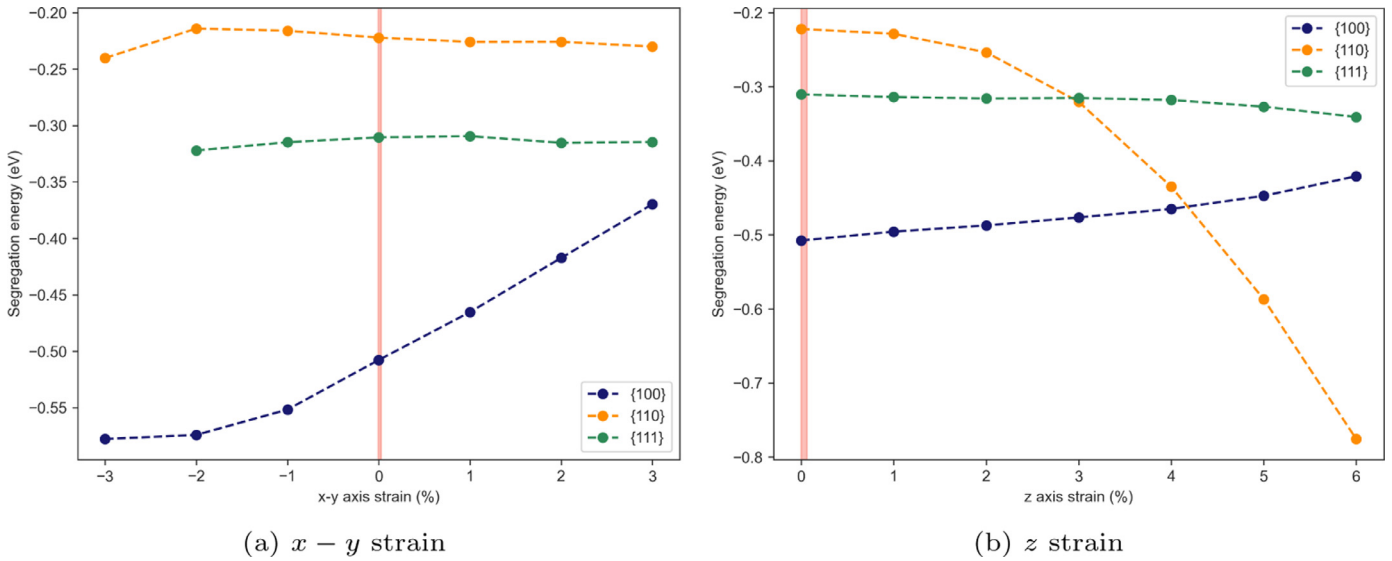

Fig. 11. Plots show the variation in calculated segregation energy of Ni to each Fe-Cu interface orientation with strain in the $x-y$ plane and in the z direction. Pink bars show the magnitude of strains expected to form at the surface of coherent Cu nanoprecipitates.

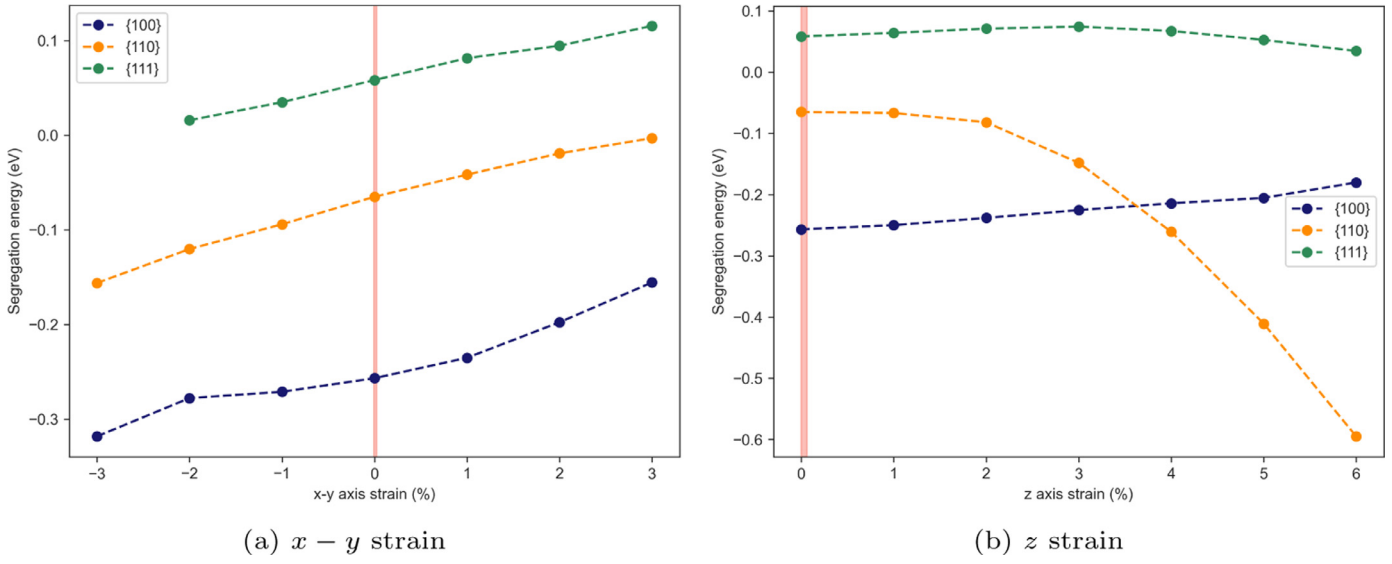

Fig. 12. Plots show the variation in calculated segregation energy of Si to each Fe-Cu interface orientation with strain in the $x-y$ plane and in the z direction. Pink bars show the magnitude of strains expected to form at the surface of coherent Cu nanoprecipitates.

Whilst the variation in calculated segregation energies may appear significant, particularly for the applied $x-y$ plane strains, it is important to note the scale of misfit strains one might expect in this plane in the region surrounding a Cu nanoprecipitate. Our previous work [43] using an embedded atom method (EAM) potential suggests the magnitude of these strains in the plane of and perpendicular to the interface are comfortably below 1% due to the small lattice mismatch (DFT predicts lattice parameters of 0.283 nm and 0.289 nm for bcc Fe and bcc Cu respectively). These narrow ranges of EAM potential predicted strains are overlaid in pink on Figs. 11 and 12 for both strain types. These realistic strain regions illustrate that in practice we would expect both the $x-y$ plane strain and z strain to have little influence on segregation energy.

If Cu nanoprecipitate size is going to influence segregation behaviour it is unlikely to do so through the strain states that surround Cu nanoprecipitate cores of different sizes due to the small strains present and the relatively weak influence of strain on segregation energy. It is instead more likely that Cu nanoprecipitate size would influence segregation behaviour through the orientation of interfaces that make up the Cu nanoprecipitate's surface. As before, in these interface strain studies a bulk solute concentration of 0.40 at.% was used for both Ni and Si.

3.4. Segregation site dependency

Whilst up to this point we have focussed on solute segregation to site 1, we now look at the influence of different segregation sites on the segregation energy calculated for Ni and Si. Figure 13 shows the segregation energy of Ni and Si to sites 1 (the on-interface site), 2, 3 and 4 (illustrated in Fig. 4) for effective bulk compositions of 0.40 at.% Ni and 0.40 at.% Si. Figure 13a shows that, in general, for Ni there is little driving force for segregation to sites away from the on-interface plane for all Fe-Cu interface orientations. It is interesting to note that for the {111} orientated Fe-Cu interface the range of attractive interaction for Ni appears to be non-zero

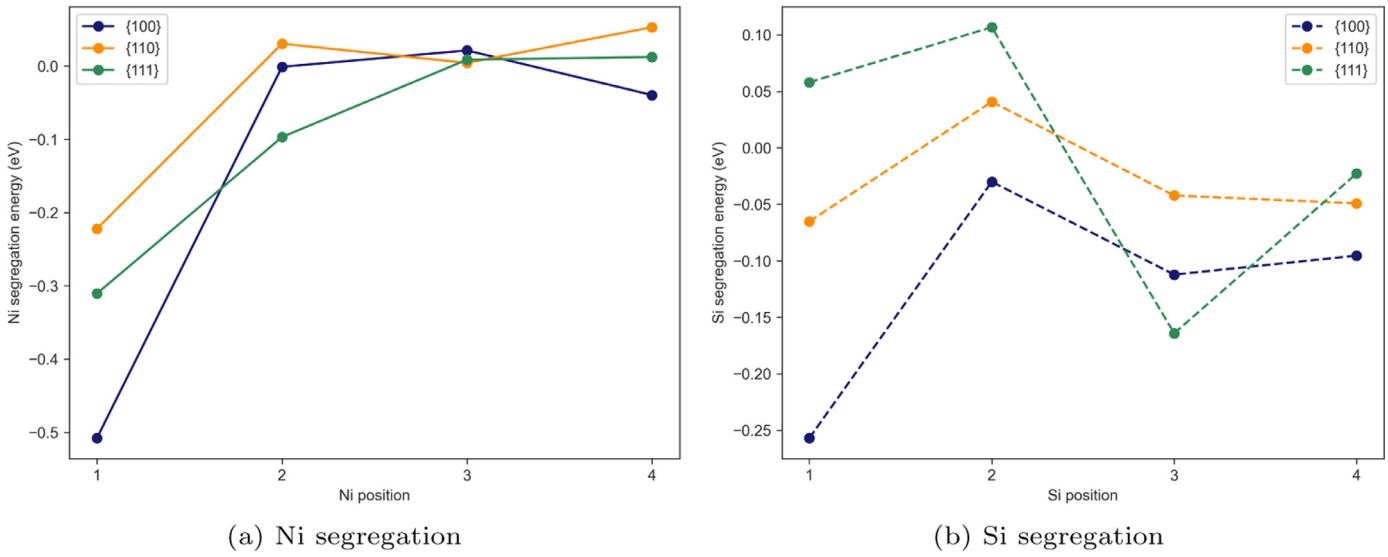

Fig. 13. Plots show the segregation energies of Ni (a) and Si (b) to interface adjacent sites (as illustrated in Fig. 4) for all three orientations of Fe-Cu interface calculated using the ERB method.

(approx. 0.16 nm) in contrast to the {100} and {110} orientations where the range of attractive interaction is effectively zero.

The segregation of Si to near interface sites is more complex as shown in Fig. 13b. There seem to be off-interface sites for all three interface orientations that energetically favour Si segregation, most notably site 3. It is interesting to observe that for the {111} orientation Si has a greater segregation energy to site 3 than to site 1 (i.e. on the interface itself). If we only consider the segregation energy of Si to the most favourable segregation sites then the relationships we see between segregation energy and interface orientation in Ni is reproduced for Si, i.e. Si segregation is strongest to the {100} orientation followed by the {111} orientation with the {110} orientation being least favourable. Unlike Ni, for Si to reach the Fe-Cu interface it may be necessary for it to pass through sites which are substantially less energetically favourable compared to those in which it previously sat. Though, in some cases solute may migrate to the interface without passing though sites sequentially. Using these energetic arguments we can envisage a scenario in which Si becomes stuck some way back from the {110} and {111} orientated Fe-Cu interfaces due to the small (or non-existent) reductions in energy associated with moving to the interface, providing little driving force for continued migration. The reason for the Si's preference for site 3 over sites 1 and 2 is likely due to two factors. Firstly, atomic sites closer to the interface are more likely to be subjected to large strains which we see from Fig. 10b substantially contribute to Si's repulsion from the {111} interface at site 1. Secondly, the number and types of bonds formed by Si at the different sites varies substantially. At site 1 in the {111} orientated Fe-Cu interface, Si forms four first nearest neighbour (1nn) bonds and three second nearest neighbour (2nn) bonds to Cu atoms. At site 2, Si forms one 1nn bond and three 2nn bonds to Cu atoms. Finally at site 3, Si forms a single 1nn bond to a Cu atom. We see from Whiting et al. [29] that the Cu-Si interaction is quite strongly attractive in the 1nn position but weakly repulsive at the 2nn position in bcc Fe. It thus seems logical from a bonding perspective that site 3 may be more energetically favourable than site 2 given they both have a single strongly attractive 1nn bond but site 2 also has 3 weakly repulsive 2nn bonds. Site 1 has four 1nn bonds and three 2nn bonds to Cu suggesting it should be more attractive than site 3. For all three interfaces we see a reduced attraction of Si to site 2 compared to sites 1 and 3 which may be attributed in all cases to the increased proportion of 2nn Si-Cu bonds compared to 1nn Si-Cu bonds and Si-Fe bonds.

It is important to note that the energy required to move between these substitutional sites has not been calculated and so segregation pathways which appear low-energy may in fact have large energy barriers associated with the movement of solute from one substitutional site to the next.

3.5. Equilibrium interface solute occupancy

Here we present our calculations of the equilibrium interface solute occupancies using the Langmuir-McLean equation [49,50]:

$$X_I^{\Phi} = \frac{X_I \exp(-E^I_{\mathrm{seg,i}}/k_{\mathrm{B}}T)}{1 + X_I[\exp(-E^I_{\mathrm{seg,i}}/k_{\mathrm{B}}T) - 1]}, \tag{6}$$

where X_I^{Φ} and X_I give the fractional occupations of available solute sites at the interface and in the lattice respectively. T is the temperature and k_{B} is Boltzmann's constant.

Figure 14 shows the change in expected interface Ni occupancy with increasing temperature for all three interface orientations. These calculations only consider segregation to on-interface sites (i.e. site 1). The range of typical RPV operating temperatures is shown by the pink region. We can see that for the {100} Fe-Cu interface in the temperature region of interest the expected Ni interface occupancy is very high and is largely unaffected by temperature or bulk Ni concentration. This is logical given the strong segregation energy associated with {100} Fe-Cu interface for Ni. More interesting are the {110} and {111} orientated Fe-Cu interfaces which show a much broader spread of predicted Ni occupancies across the temperature range and also with bulk Ni concentration. It is evident from Fig. 14 that pressure vessel steels lower in Ni (such as A508-3, approx. 0.37–0.93 at.%Ni) are likely to see considerably lower Ni occupancies at Fe-Cu interfaces with {110} and {111} orientations compared to higher Ni pressure vessel steels (like A508-4N, approx. 2.60–3.61 at.%Ni) at typical RPV operating temperatures. This finding is significant given that our earlier work [43] has indicated that much of a Cu nanoprecipitate's surface is likely to be made up of the {110} due to its relatively low interfacial energy density.

In order to better understand how bulk Ni concentration influences segregation behaviour, two steels compositions from ASTM A508 have been investigated (Grade 3 and Grade 4N) [58]. We performed a linear interpolation between our calculated bulk Ni con-

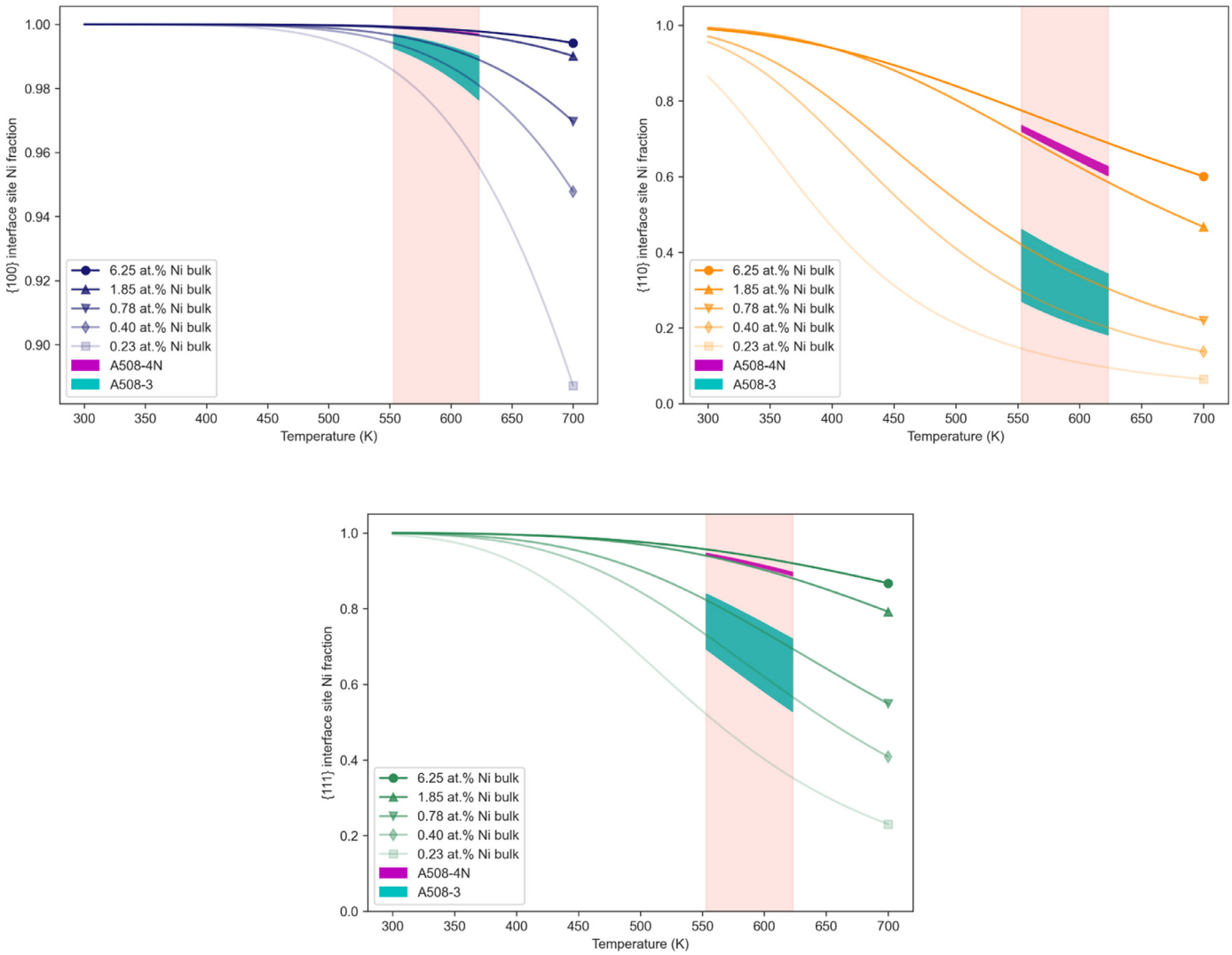

Fig. 14. Plots show the Ni fractional occupation of sites on the {100}, {110} and {111} orientated Fe-Cu interfaces with increasing temperature for different effective bulk Ni concentrations where the different effective bulk Ni concentrations are illustrated by the line colours. Approximate RPV operating temperatures are shown in pink. Ni composition ranges for pressure vessel steel grades A508-4N (magenta) and A508-3 (cyan) are also shown. Note the *y* axis scale for the {100} orientation is reduced to better illustrate the variations with respect to bulk Ni concentration. (For interpretation of the references to color in this figure legend, the reader is referred to the web version of this article.)

centrations to plot the expected interfacial Ni occupancies across the region bound by the lower and upper Ni limits for both grades as specified by the ASTM standard across the temperature range of interest. These interpolated regions are shown in cyan for A508-3 and magenta for A508-4N on Fig. 14. For all three interface orientations we see that variations in the bulk Ni concentration for A508-4N steels result in only small changes to the expected interfacial solute occupancy (< 0.05 in all cases). However, for A508-3 steels these differences are more pronounced with low levels of Ni alloying resulting in interfacial solute occupancies 0.1–0.2 lower than the high Ni examples for the {110} and {111} orientations across the operational temperature range. This suggests that two RPVs, whilst both nominally made of A508-3 steel, may see relatively large variations in the amount of Ni that segregates to Cu nano-precipitates dependent on their specific Ni contents.

Similarly to the case for Ni, Fig. 15 shows the change in expected interface Si occupancy with increasing temperature. Note that rising temperature leads to increases in the concentration of Si at the {111} interfaces because segregation is energetically disfavoured for this orientation. For the {100} Fe-Cu interface there is a substantial spread of expected interface Si occupancy in the temperature range of interest and the bulk Si concentrations explored. This spread is particularly pronounced for the lower bulk Si concentration data, which is of particular interest due to the relatively low Si content in A508-3 and A508-4N steels (0.28–0.74 at.% in both A508-3 and A508-4N), suggesting relatively small changes in bulk Si composition can substantially alter the Si segregation one would expect to the {100} orientated interface. The significance of this is likely to be more prominent in determining the likelihood of Si-rich appendages forming from a small area of {100} orientated interface. The interface Si occupancies of the {110} and {111} orientated Fe-Cu interfaces appear to be considerably less sensitive to temperature and bulk Si content with both interfaces expected to possess relatively low Si occupancies for typical bulk Si contents.

As before, linear interpolations were performed to indicate the lower and upper limits of Si contents for A508-3 and A508-4N steels as specified by the ASTM standard [58] which bound the region highlighted in cyan on Fig. 15. For the {110} and {111} these differences in bulk Si concentration between the steel grades result in only minor changes (< 0.03) to the predicted interfacial Si occupancy in the temperature range of interest. In contrast, for the {100} orientation the bulk Si concentration results in a much larger

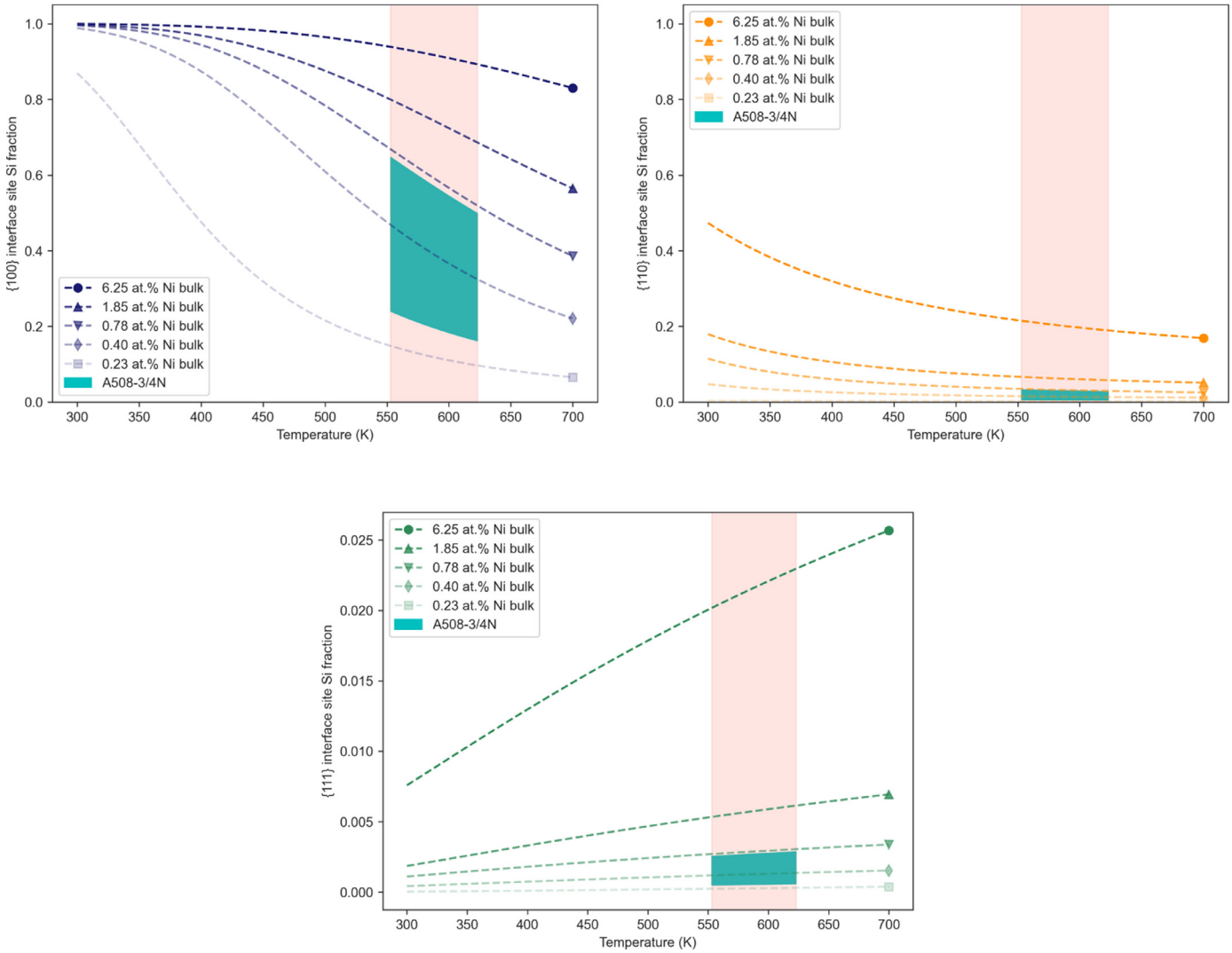

Fig. 15. Plots show the Si fractional occupation of sites on the {100}, {110} and {111} orientated Fe-Cu interfaces with increasing temperature for different effective bulk Si concentrations where the different effective bulk Si concentrations are illustrated by the line colours. Si composition ranges for pressure vessel steel grades A508-4N and A508-3 are shown in cyan. Approximate RPV operating temperatures are shown in pink. Note the *y* axis scale for the {111} orientation is reduced due to the very low interfacial solute occupations predicted. (For interpretation of the references to color in this figure legend, the reader is referred to the web version of this article.)

variation of the predicted interfacial solute occupancy (0.3–0.4) across the temperature range of interest. As previously mentioned, the significance of this is likely confined to the composition of appendage structures. It is important to note that in Section 3.4 we commented that site 3 appears to have a more attractive segregation energy than site 1 for the {111} orientated Fe-Cu interface. If we were to treat this finding as accurate and use the segregation energy of Si to site 3 in our interfacial solute occupancy calculation the bulk Si composition has a much stronger influence. This change results in variations in the predicted interfacial Si occupation fraction for the {111} orientation of 0.1–0.2 between the low and high Si limits for both grades in the operational temperature range. This plot is included in Appendix C as Fig. C.1.

We note that the results in Figs. 14 and 15 are based on the interfacial solute concentration for binary systems at thermal equilibrium and do not take into account irradiation effects, which may contribute substantially to the segregation behaviour of these systems, or the influence of other segregants.

4. Conclusions

We find that for the segregation of Ni to Fe-Cu interfaces the use of an external reference bulk (ERB) method gives similar levels of convergence to the internal reference bulk (IRB) method but requires smaller simulation cells. Whilst in this particular application the ERB method proved superior due to the reusability of many calculated values it is important to note that if only a small number of systems are to be investigated the IRB method may well prove more efficient. We then used the ERB method to investigate the segregation of Ni and Si to {100}, {110} and {111} orientated coherent Fe-Cu interfaces. The key conclusions of this work are:

- Higher interfacial solute concentrations for both solute species generally result in less attractive segregation energies for the {100} orientated Fe-Cu interface though this effect is less apparent for the {110} and {111} orientations.
- Ni is attracted to all three interface orientations in the dilute limit with a preference for the {100} and {111} orientations compared to the {110} orientation. There is very little dependence of Ni's segregation energy on bulk Ni concentration and

the majority of Ni's attraction to Fe-Cu interface's seems to derive from chemical, rather than elastic, effects.
- For dilute interfaces Si is somewhat attracted to the {100} orientated Fe-Cu interface, very weakly attracted to the {110} orientated interface and weakly repelled by the {111} orientated interface. Si segregation displays a stronger dependence on bulk Si concentration, compared to Ni, with more attractive segregation energies calculated at higher bulk Si concentrations. The elastic and chemical contributions to segregation energy are more balanced than in the case of Ni resulting in smaller segregation energy values. The elastic contribution is typically positive (and so repulsive) whilst the chemical contribution is negative (and so attractive).
- In general, strain in the interface has a relatively weak influence on the segregation energies calculated. As such, if the size of Cu nanoprecipitates influence segregation behaviour it is likely that they do so through the interface orientations that make up their surfaces rather than the strain states that surround them.
- When applying the ERB method to interface-adjacent segregation sites we observe that for Ni, the {111} orientated Fe-Cu exhibits a comparatively long range attraction with near-interface sites becoming increasingly attractive as the distance between the solute and interface reduces. This trend is not observed for the {100} and {110} orientated interfaces where near-interface sites typically have segregation energies close to zero.
- When applying the ERB method to Si in near-interface sites we observe that for the {111} orientation there is a strong preference for segregation to site 3 compared to sites 1 and 2. The segregation of Si to the {110} interface exhibits similar, though less pronounced, behaviour with a relatively small difference in segregation energy to be found between sites 1 and 3. This may suggest Si preferentially segregates to near-interface sites rather than to the interface plane itself in some cases.
- Using the Langmuir-McLean binary isotherm equation [49,50] we predict that for Ni, RPV operating temperatures and bulk Ni compositions may substantially alter the expected Ni concentration of {110} and {111} orientated Fe-Cu interfaces. Interfacial Si concentration appears to be less sensitive to bulk Si composition and temperature. However, for the {100} orientated Fe-Cu interface, changes in the bulk Si concentration can yield substantial variations in interface composition.
- Using this approach and ASTM pressure vessel specifications we estimate that at conventional RPV operating temperatures the use of a relatively high-Ni A508-3 steel may result in an interfacial Ni occupancy fraction up to 0.2 greater than a low-Ni A508-3 steel. Similarly, a relatively high-Si A508-3/4N steel could result in interfacial Si occupation fractions up to 0.4 greater than the low-Si limit.

Acknowledgements

AMG would like to thank Rolls-Royce plc and EPSRC grant EP/L016273 Centre for Doctoral Training in Advanced Metallic Systems for supporting this research. The authors would like to acknowledge the assistance given by Research IT, the use of the Computational Shared Facility and the use of The HPC Pool funded by the Research Lifecycle Programme at The University of Manchester. The authors are additionally grateful to the Computational Materials Design group at the Max-Planck-Institut für Eisenforschung (MPIE) and the NEUIRR Steels group for their invaluable assistance with this research. CPR was funded by a University Research Fellowship of the Royal Society.

Appendix A. Simulation cell sizes

Table A1
Effective bulk solute concentrations (C_B) for the different sizes of reference bulk simulation cells used in ERB method calculations.

Unit cells in ($x \times y \times z$)	C_B (at.%)
$2 \times 2 \times 2$	6.250
$3 \times 3 \times 3$	1.852
$4 \times 4 \times 4$	0.781
$5 \times 5 \times 5$	0.400
$6 \times 6 \times 6$	0.231

Table A2
Simulation cell sizes for interfacial spacing convergence study.

Interface orientation	No. atoms	Cell length (nm)
{100}	12	1.700
	16	2.267
	24	3.401
	32	4.534
	48	6.802
{110}	16	1.603
	32	3.206
	48	4.809
	64	6.413
	80	8.016
{111}	24	1.963
	36	2.945
	48	3.927
	60	4.909
	72	5.890

Table A3
Simulation cell arrays for interfacial solute concentration convergence study.

Interface orientation	Γ_B (at · nm^{-2})	$x \times y$ cell array	No. atoms	Min. solute spacing (nm)
{100}	12.45	1×1	16	0.283
	3.11	2×2	64	0.567
	1.38	3×3	144	0.850
	0.78	4×4	256	1.137
	0.50	5×5	400	1.417
{110}	8.80	1×1	32	0.283
	2.20	2×2	128	0.567
	0.98	3×3	288	0.850
	0.55	4×4	512	1.417
{111}	7.19	1×1	24	0.401
	1.80	2×2	96	0.802
	0.80	3×3	216	1.202
	0.50	4×4	384	1.603

Appendix B. IRB additional derivation

See Section 2 for definitions of the symbols.

$$\begin{aligned} E^{\mathrm{I,IRB}}_{\mathrm{seg,i}} &= E^{\mathrm{I,ERB}}_{\mathrm{seg,i}} - E^{\mathrm{I,ERB}}_{\mathrm{seg,b}} \\ &= [(E^{\mathrm{FeICu}}_{\mathrm{i}} - E^{\mathrm{FeCu}}_{\mathrm{i}}) - (E^{\mathrm{FeI}}_{\mathrm{B}} - E^{\mathrm{Fe}}_{\mathrm{B}})] \\ &\quad -[(E^{\mathrm{FeICu}}_{\mathrm{b}} - E^{\mathrm{FeCu}}_{\mathrm{b}}) - (E^{\mathrm{FeI}}_{\mathrm{B}} - E^{\mathrm{Fe}}_{\mathrm{B}})] \\ &= (E^{\mathrm{FeICu}}_{\mathrm{i}} - E^{\mathrm{FeCu}}_{\mathrm{i}}) - (E^{\mathrm{FeICu}}_{\mathrm{b}} - E^{\mathrm{FeCu}}_{\mathrm{b}}), \end{aligned} \tag{B.1}$$

which becomes

$$E^{\mathrm{I,IRB}}_{\mathrm{seg,i}} = E^{\mathrm{FeICu}}_{\mathrm{i}} - E^{\mathrm{FeICu}}_{\mathrm{b}} \tag{B.2}$$

as before (i.e. the IRB method Eq. (1)), given $E^{\mathrm{FeCu}}_{\mathrm{i}} = E^{\mathrm{FeCu}}_{\mathrm{b}}$.

Appendix C. Equilibrium interface solute occupancy

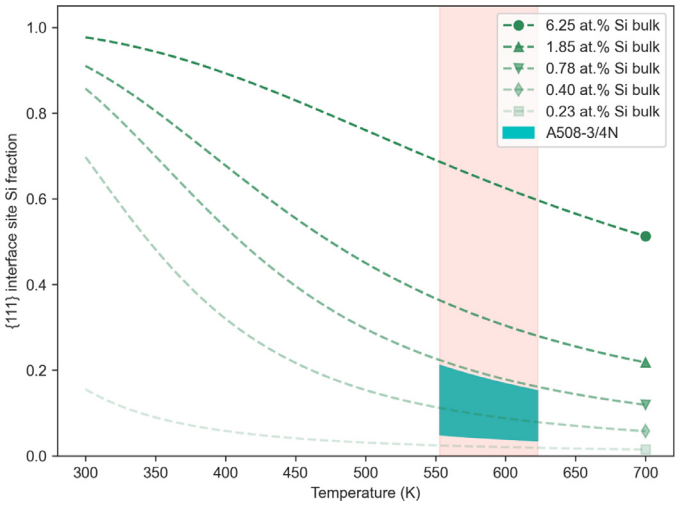

Fig. C1. Plot shows the Si fractional occupation of site 3 near to the {111} orientated Fe-Cu interfaces with increasing temperature for different effective bulk Si concentrations. Site 3 was calculated to be more attractive to Si segregation compared to the on-interface position (site 1).

References

[1] U. Potapovs, J.R. Hawthorne, The effect of residual elements on the response of selected pressure-vessel steels and weldments to irradiation at 550 °F, Nucl. Appl. 6 (1) (1969) 27–46.

[2] G.R. Odette, On the dominant mechanism of irradiation embrittlement of reactor pressure vessel steels, Scr. Metall. 17 (10) (1983) 1183–1188, doi:10.1016/0036-9748(83)90280-6.

[3] D. Isheim, R.P. Kolli, M.E. Fine, D.N. Seidman, An atom-probe tomographic study of the temporal evolution of the nanostructure of Fe-Cu based high-strength low-carbon steels, Scr. Mater. 55 (1 SPEC. ISS.) (2006) 35–40, doi:10.1016/j.scriptamat.2006.02.040.

[4] K. Osamura, H. Okuda, K. Asano, M. Furusaka, K. Kishida, F. Kurosawa, R. Uemori, SANS Study of phase decomposition in Fe-Cu alloy with Ni and Mn addition, ISIJ Int. 34 (4) (1994) 346–354.

[5] P.D. Styman, J.M. Hyde, K. Wilford, A. Morley, G.D. Smith, Precipitation in long term thermally aged high copper, high nickel model RPV steel welds, Prog. Nucl. Energy 57 (2012) 86–92, doi:10.1016/j.pnucene.2011.10.010.

[6] P.D. Styman, J.M. Hyde, K. Wilford, D. Parfitt, N. Riddle, G.D. Smith, Characterisation of interfacial segregation to Cu-enriched precipitates in two thermally aged reactor pressure vessel steel welds, Ultramicroscopy 159 (2015) 292–298, doi:10.1016/j.ultramic.2015.05.013.

[7] S. Shu, B.D. Wirth, P.B. Wells, D.D. Morgan, G.R. Odette, Multi-technique characterization of the precipitates in thermally aged and neutron irradiated Fe-Cu and Fe-Cu-Mn model alloys: atom probe tomography reconstruction implications, Acta Mater. 146 (2018) 237–252, doi:10.1016/j.actamat.2017.12.006.

[8] S. Shu, N. Almirall, P.B. Wells, T. Yamamoto, G.R. Odette, D.D. Morgan, Precipitation in Fe-Cu and Fe-Cu-Mn model alloys under irradiation: dose rate effects, Acta Mater. 157 (2018) 72–82, doi:10.1016/j.actamat.2018.07.017.

[9] M. Miller, B. Wirth, G. Odette, Precipitation in neutron-irradiated Fe–Cu and Fe–Cu–Mn model alloys: a comparison of APT and SANS data, Mater. Sci. Eng. A 353 (1–2) (2003) 133–139, doi:10.1016/S0921-5093(02)00679-2.

[10] M.K. Miller, K.F. Russell, Embrittlement of RPV steels: an atom probe tomography perspective, J. Nucl. Mater. 371 (1–3) (2007) 145–160, doi:10.1016/j.jnucmat.2007.05.003.

[11] S. Shu, P.B. Wells, N. Almirall, G.R. Odette, D.D. Morgan, Thermodynamics and kinetics of core-shell versus appendage co-precipitation morphologies: an example in the Fe-Cu-Mn-Ni-Si system, Acta Mater. 157 (2018) 298–306, doi:10.1016/j.actamat.2018.07.037.

[12] C.L. Liu, G.R. Odette, B.D. Wirth, G.E. Lucas, A lattice Monte Carlo simulation of nanophase compositions and structures in irradiated pressure vessel Fe-Cu-Ni-Mn-Si steels, Mater. Sci. Eng., A 238 (1) (1997) 202–209, doi:10.1016/S0921-5093(97)00450-4.

[13] G.R. Odette, B. Wirth, A computational microscopy study of nanostructural evolution in irradiated pressure vessel steels, J. Nucl. Mater. 251 (1997) 157–171, doi:10.1016/S0022-3115(97)00267-5.

[14] O.I. Gorbatov, Y.N. Gornostyrev, P.A. Korzhavyi, A.V. Ruban, Effect of Ni and Mn on the formation of Cu precipitates in α-Fe, Scr. Mater. 102 (2015) 11–14, doi:10.1016/j.scriptamat.2015.01.016.

[15] G.R. Odette, G.E. Lucas, Recent progress in understanding reactor pressure vessel steel embrittlement, 144, 1998, doi:10.1080/10420159808229676.

[16] M.K. Miller, M.A. Sokolov, R.K. Nanstad, K.F. Russell, APT characterization of high nickel RPV steels, J. Nucl. Mater. 361 (351) (2006) 187–196, doi:10.1016/j.jnucmat.2006.12.015.

[17] P.B. Wells, T. Yamamoto, B. Miller, T. Milot, J. Cole, Y. Wu, G.R. Odette, Evolution of manganese-nickel-silicon-dominated phases in highly irradiated reactor pressure vessel steels, Acta Mater. 80 (2014) 205–219, doi:10.1016/j.actamat.2014.07.040.

[18] G.R. Odette, G.E. Lucas, Embrittlement of nuclear reactor pressure vessels, J. Miner. Metals Mater. Soc. 53 (7) (2001) 18–22, doi:10.1007/s11837-001-0081-0.

[19] D.J.M. King, P.A. Burr, S.C. Middleburgh, T.M. Whiting, M.G. Burke, M.R. Wenman, The formation and structure of Fe-Mn-Ni-Si solute clusters and G-phase precipitates in steels, J. Nucl. Mater. 505 (2018) 1–6, doi:10.1016/j.jnucmat.2018.03.050.

[20] G. Bonny, D. Terentyev, A. Bakaev, E.E. Zhurkin, M. Hou, D. Van Neck, L. Malerba, On the thermal stability of late blooming phases in reactor pressure vessel steels: an atomistic study, J. Nucl. Mater. 442 (1–3) (2013) 282–291, doi:10.1016/j.jnucmat.2013.08.018.

[21] P.D. Edmondson, C.M. Parish, R.K. Nanstad, Using complimentary microscopy methods to examine Ni-Mn-Si-precipitates in highly-irradiated reactor pressure vessel steels, Acta Mater. 134 (2017) 31–39, doi:10.1016/j.actamat.2017.05.043.

[22] R.P. Kolli, Z. Mao, D.N. Seidman, D.T. Keane, Identification of a $Ni_{0.5}$ ($Al_{0.5-x}$ Mn_x) B2 phase at the heterophase interfaces of Cu-rich precipitates in an α-Fe matrix, Appl. Phys. Lett. 91 (24) (2007), doi:10.1063/1.2820378.

[23] G.R. Odette, R.K. Nanstad, Predictive reactor pressure vessel steel irradiation embrittlement models: issues and opportunities, J. Miner. Metals Mater. Soci. 61 (7) (2009) 17–23, doi:10.1007/s11837-009-0097-4.

[24] P.J. Othen, M.L. Jenkins, G.D.W. Smith, High-resolution electron microscopy studies of the structure of cu precipitates in α-Fe, Philos. Mag. A 70 (1) (1994) 1–24, doi:10.1080/01418619408242533.

[25] P.D. Styman, J.M. Hyde, D. Parfitt, K. Wilford, M.G. Burke, C.A. English, P. Efsing, Post-irradiation annealing of Ni–Mn–Si-enriched clusters in a neutron-irradiated RPV steel weld using atom probe tomography, J. Nucl. Mater. 459 (2015) 127–134, doi:10.1016/j.jnucmat.2015.01.027.

[26] A. Wagner, F. Bergner, R. Chaouadi, H. Hein, M. Hernández-Mayoral, M. Serrano, A. Ulbricht, E. Altstadt, Effect of neutron flux on the characteristics of irradiation-induced nanofeatures and hardening in pressure vessel steels, Acta Mater. 104 (2016) 131–142, doi:10.1016/j.actamat.2015.11.027.

[27] A.T. Al-Motasem, M. Posselt, F. Bergner, Nanoclusters in bcc-Fe containing vacancies, copper and nickel: structure and energetics, J. Nucl. Mater. 418 (1–3) (2011) 215–222, doi:10.1016/j.jnucmat.2011.07.002.

[28] L. Messina, M. Nastar, T. Garnier, C. Domain, P. Olsson, Exact ab initio transport coefficients in bcc Fe-X (X=Cr, Cu, Mn, Ni, P, Si) dilute alloys, Phys. Rev. B 90 (10) (2014) 1–15, doi:10.1103/PhysRevB.90.104203.

[29] T.M. Whiting, P.A. Burr, D.J. King, M.R. Wenman, Understanding the importance of the energetics of Mn, Ni, Cu, Si and vacancy triplet clusters in bcc Fe, J. Appl. Phys. 126 (11) (2019), doi:10.1063/1.5109483.

[30] Y. Zhang, P.C. Millett, M.R. Tonks, X.M. Bai, S.B. Biner, Preferential Cu precipitation at extended defects in bcc Fe: an atomistic study, Comput. Mater. Sci 101 (2015) 181–188, doi:10.1016/j.commatsci.2015.01.041.

[31] Y.P. Xie, S.J. Zhao, First principles study of Al and Ni segregation to the α-Fe/Cu (1 0 0) coherent interface and their effects on the interfacial cohesion, Comput. Mater. Sci 63 (2012) 329–335, doi:10.1016/j.commatsci.2012.06.036.

[32] Y.P. Xie, S.J. Zhao, The segregation behavior of manganese and silicon at the coherent interfaces of copper precipitates in ferritic steels, J. Nucl. Mater. 445 (1–3) (2014) 43–49, doi:10.1016/j.jnucmat.2013.10.054.

[33] P. Lejček, M. Všianská, M. Šob, Recent trends and open questions in grain boundary segregation, J. Mater. Res. 33 (18) (2018) 2647–2660, doi:10.1557/jmr.2018.230.

[34] H. Guesmi, C. Louis, L. Delannoy, Chemisorbed atomic oxygen inducing Pd segregation in PdAu(111) alloy: energetic and electronic DFT analysis, Chem. Phys. Lett. 503 (2011) 97–100.

[35] A. Lindman, E.E. Helgee, G. Wahnström, Theoretical modeling of defect segregation and space-charge formation in the BaZr03 (210)[001] tilt grain boundary, Solid State Ionics 252 (2013) 121–125.

[36] D. Shin, A. Shyam, S. Lee, Y. Yamamoto, J.A. Haynes, Solute segregation at the Al/θ-Al2Cu interface in Al-Cu alloys, Acta Mater. 141 (2017) 327–340.

[37] L. Huber, J. Rottler, M. Militzer, Atomistic simulations of the interaction of alloying elements with grain boundaries in Mg, Acta Mater. 80 (2014) 194–204, doi:10.1016/j.actamat.2014.07.047.

[38] L. Huber, B. Grabowski, M. Militzer, J. Neugebauer, J. Rottler, Ab initio modelling of solute segregation energies to a general grain boundary, Acta Mater. 132 (2017) 138–148, doi:10.1016/j.actamat.2017.04.024.

[39] D. Scheiber, L. Romaner, R. Pippan, P. Puschnig, Impact of solute-solute interactions on grain boundary segregation and cohesion in molybdenum, Phys. Rev. Mater. 2 (9) (2018) 1–13, doi:10.1103/PhysRevMaterials.2.093609.

[40] R. Tran, Z. Xu, N. Zhou, B. Radhakrishnan, J. Luo, S.P. Ong, Computational study of metallic dopant segregation and embrittlement at molybdenum grain boundaries, Acta Mater. 117 (2016) 91–99.

[41] J. Zhang, Y. Dou, Y. Zheng, Twin-boundary segregation energies and solute-diffusion activation enthalpies in Mg-based binary systems: afirst-principles study, Scr. Mater. 80 (2014) 17–20.

[42] M.S. Daw, M.I. Baskes, Embedded-atom method: derivation and application to impurities, surfaces, and other defects in metals, Phys. Rev. B 29 (12) (1984) 6443–6453.

[43] A.M. Garrett, C.P. Race, Cu nanoprecipitate morphologies and interfacial energy densities in bcc Fe from density functional theory (DFT), Comput. Mater. Sci 188 (2021), doi:10.1016/j.commatsci.2020.110149.
[44] G. Kresse, J. Furthmüller, Efficient iterative schemes for ab initio total-energy calculations using a plane-wave basis set, Phys. Rev. B 54 (16) (1996) 169–186.
[45] G. Kresse, D. Joubert, From ultrasoft pseudopotentials to the projector augmented-wave method, Phys. Rev. B 59 (3) (1999) 1758–1775, doi:10.1103/PhysRevB.59.1758.
[46] J.P. Perdew, K. Burke, M. Ernzerhof, Generalized gradient approximation made simple, Phys. Rev. Lett. 77 (18) (1996) 3865–3868.
[47] M. Methfessel, A.T. Paxton, High-precision sampling for Brillouin-zone integration in metals, Phys. Rev. B 40 (6) (1989) 3616–3621, doi:10.1103/PhysRevB.40.3616.
[48] H.J. Monkhorst, J.D. Pack, Special points for Brillouin-zone integration Monkhorst and Pack, Phys. Rev. B 13 (12) (1976) 5188–5192.
[49] D. McLean, Grain Boundaries in Metals, Clarendon Press, Oxford, 1957.
[50] M.P. Seah, Grain boundary segregation, J. Phys. F 10 (1980) 1043–1064.
[51] P. Lejček, Grain Boundary Segregation in Metals, vol. 136, Springer, Berlin, 2010, doi:10.1007/978-3-642-12505-8_1.
[52] A. Bakaev, D. Terentyev, X. He, D. Van Neck, Synergetic effects of Mn and Si in the interaction with point defects in bcc Fe, J. Nucl. Mater. 455 (1–3) (2014) 5–9, doi:10.1016/j.jnucmat.2014.02.033.
[53] M.K. Miller, K.A. Powers, R.K. Nanstad, P. Efsing, Atom probe tomography characterizations of high nickel, low copper surveillance RPV welds irradiated to high fluences, J. Nucl. Mater. 437 (1–3) (2013) 107–115, doi:10.1016/j.jnucmat.2013.01.312.
[54] C.D. Versteylen, N.H. Van Dijk, M.H. Sluiter, First-principles analysis of solute diffusion in dilute bcc Fe- X alloys, Phys. Rev. B 96 (9) (2017) 1–13, doi:10.1103/PhysRevB.96.094105.
[55] K. Hirano, M. Cohen, B.L. Averbach, Diffusion of nickel into iron, Acta Metall. 9 (5) (1961) 440–445, doi:10.1016/0001-6160(61)90138-9.
[56] R.J. Borg, D.Y. Lai, The diffusion of gold, nickel, and cobalt in alpha iron: a study of the effect of ferromagnetism upon diffusion, Acta Metall. 11 (8) (1963) 861–866, doi:10.1016/0001-6160(63)90055-5.
[57] D. Bergner, Y. Khaddour, S. Lörx, Diffusion of Si in bcc- and fcc-Fe, Defect Diffusion Forum 66–69 (1990) 1407–1412, doi:10.4028/www.scientific.net/DDF.66-69.1407.
[58] A.S.T.M. Standard, Standard specification for quenched and tempered vacuum-treated carbon and alloy steel forgings for pressure vessels - A508/A508M-18, 2018, doi:10.1520/A0508.